Production and characterisation of bacterial cellulose hydrogels loaded with curcumin encapsulated in cyclodextrins as wound dressings

A. Gupta[a,c*], D. J. Keddie[b], V. Kannappan[c], H. Gibson[b,c], I. R. Khalil[b], M. Kowalczuk[b,c,e], C. Martin[d], X. Shuai[f], I. Radecka[b,c*]

[a]School of Pharmacy, Faculty of Science and Engineering, University of Wolverhampton, Wulfruna Street, Wolverhampton,WV1 1LY, UK.
[b]Wolverhampton School of Sciences, Faculty of Science and Engineering, University of Wolverhampton, Wulfruna Street, Wolverhampton, WV1 1LY, UK.
[c]Research Institute in Healthcare Science, Faculty of Science and Engineering, University of Wolverhampton, Wulfruna Street, Wolverhampton, WV1 1LY, UK.
[d]Department of Biological Sciences, Institute of Science and the Environment, University of Worcester, WR2 6AJ, UK.
[e]Centre of Polymer and Carbon Materials, Polish Academy of Sciences, M. Curie-Sklodowskiej 34, 41-819 Zabrze, Poland.
[f]PCFM Lab of Ministry of Education, School of Materials Science and Engineering, Sun Yat-sen University, Guangzhou 510275, China

[*]Corresponding authors: a.gupta@wlv.ac.uk , I.Radecka@wlv.ac.uk

Keywords: Biosynthetic hydrogel, Curcumin, Cyclodextrin, Antimicrobial, Antioxidant, Wound management

Highlights

- Curcumin:cyclodextrin-loaded cellulose based biosynthetic hydrogels were produced.
- These novel hydrogels exhibited haemocompatibility and cellular biocompatibility.
- CUR:HPβCD-loaded-bacterial cellulose showed antibacterial and antioxidant properties.
- Acute and chronic wounds could benefit from their application.

Abstract

Natural bioactive materials with wound healing properties such as curcumin are attracting interest due to the emergence of resistant bacterial strains. The hydrophobicity of curcumin has been counteracted by using solubility enhancing cyclodextrins. Hydrogels facilitate wound healing due to unique properties and 3D network structures which allows encapsulation of healing agents. In this study, biosynthetic cellulose produced by *Gluconacetobacter xylinus* (ATCC 23770) was loaded with water soluble curcumin:hydroxypropyl-β-cyclodextrin supramolecular inclusion complex produced by a solvent evaporation method to synthesise hydrogel dressings. The ratios of solvents to solubilise curcumin and hydroxypropyl-β-cyclodextrin were tested for the production of the inclusion complex with optimum encapsulation efficacy. The results confirmed that hydroxypropyl-β-cyclodextrin enhanced the aqueous solubility of curcumin and allowed loading into bacterial cellulose hydrogels. These hydrogels were characterised for wound management applications and exhibited haemocompatability, cytocompatability, anti-staphylococcal and antioxidant abilities and therefore support the potential use of the curcumin:hydroxypropyl-β-cyclodextrin-loaded-bacterial cellulose as hydrogel dressings.

1. Introduction

Wound healing is a complex physiological process involving sequential yet overlaying phases [1,2]. Correct clinical management of wounds is vital to minimise complications during the healing process. The mandatory wound management requirements for all wounds, no matter whether they are acute or chronic, involve control of infection, cleaning the wound site and making it free from foreign material and necrotic tissue and the selection of appropriate wound dressings [3]. Passive dressings *e.g.* gauze and tulle, undoubtedly are inexpensive and provide a dry protective barrier, but cannot effectively interact and respond to changing wound conditions [4]. An ideal dressing not only covers and protects the affected area, but also optimises the wound environment to facilitate healing [3,]. George Winter in 1960s established that the optimum moisture at the wound site increases reepithelialisation and promotes healing [5]. This research revolutionised the field of wound management, and the focus of wound dressings changed from conventional dry passive products, to responsive moisture-promoting materials [4,5]. Following these research findings, a wide range of dressings based on the moist healing concept were developed with a range of different material compositions.

Hydrogels are one of the most promising candidates amongst the category of advanced moist wound dressings. Hydrogels are composed of over 90% water [6] which is responsible for their soft and malleable texture. In addition to acting as a barrier, hydrogels facilitate healing by donating moisture in the case of dry necrotic wounds and absorbing excessive exudate in the case of exudative wounds. This feature makes them capable of creating the moist micro-climate between the wound bed and the dressing at the wound site. Moreover, hydrogels reduce pain as a result of the cooling effect, allows exchange of gases and can be loaded with antimicrobials and other healing agents [6,7].

Several cross-linked natural polymers like alginate, carboxymethyl cellulose, collagen, chitosan and hyaluronic acid are in use as base materials for hydrogel dressings [1,8]. Bacterial cellulose (BC), a biosynthetic cellulose based polymeric hydrogel synthesised by *Gluconacetobacter xylinus* has attracted wide interest in biomedical applications [9]. Its hydrophilicity, biocompatibility, non-pyrogenic, high wet strength and transparency are some of the desirable properties that resulted in its use for fabrication of several proprietary wound dressings (XCell®, Bioprocess®, Dermafill™, Gengiflex® and Biofill®) [7,9] with the clinical rationale being to facilitate autolytic debridement. BC's cross-linked fibre network structure creates pores which allow impregnation of several healing agents [7].

Natural products like curcumin (CUR), the curcuminoid present in turmeric, are becoming more popular for regenerative medicine and wound management. CUR has multifaceted

mechanisms of action on wound healing [10] and less likely than presently used antibiotics to develop resistant strains [11]. CUR (diferuloylmethane) (Fig. S1a in the supporting information) is a naturally derived low molecular weight polyphenolic compound well known for its pharmacological benefits like, but not limited to, anti-inflammatory, anti-infective and anti-oxidant activities [10,11]. However, its hydrophobicity [11,12] limits its biological activity for topical delivery for wound management applications.

Microencapsulation of medicinal substances in a suitable carrier is a common practice in pharmaceutics for drug delivery. Encapsulation can be used to protect the active compound from the external environment, controlling delivery or to enhance the aqueous solubility of the hydrophobic bioactive materials [13]. Cyclodextrins (CDs) are naturally occurring cyclic oligosaccharide obtained from starch by enzymatic cyclisation that are recognized as pharmaceutical adjuvants [14,15]. There are three commonly used native cyclodextrins: α- cyclodextrin, β- cyclodextrin and γ- cyclodextrin with six, seven and eight D-glucopyranose units linked by α-1,4 glycosidic bonds respectively. These linkages of glucopyranose units result in truncated cone structures (Fig. S1b in the supporting information). The primary and secondary hydroxyl groups located at the edges are responsible for hydrophilic exterior surface of CDs. The skeletal carbons (C_3 and C_5) and endocyclic acetal oxygen of glucose residues are oriented inside which imparts a hydrophobic character to the interior CD cavity [16]. The polarity of the CD cavity has been reported to be similar to an aqueous ethanolic solution [15]. Apart from naturally occurring CDs, several chemically modified derivatives have been synthesized to improve the properties (aqueous solubility, toxicological profiles *etc.*) of native CDs [15,17].

There are several studies reported on the enhancement of aqueous solubility of lipophilic compounds by their inclusion in the CD cavity [12,13,18,19]. This can be achieved by several techniques like co-precipitation, hot melt extrusion, solvent evaporation, freeze drying, spray drying, slurry mixing, dry mixing *etc.* [14]. This study was conducted with the aim of producing novel biosynthetic hydrogel dressings with healing properties. The set objective was approached by encapsulation of CUR within hydroxypropyl-β-cyclodextrin (HPβCD) to enhance its aqueous solubility leading to consistent loading in the biosynthetic BC hydrogel matrix. The potential healing properties and the physical performance characteristics of the CUR:HPβCD-loaded-BC hydrogels were investigated.

Herein, we describe the production of CUR:HPβCD-loaded-BC hydrogels for wound management applications. Moreover, we discuss the effect of varied volume ratio of solvents to dissolve CUR and HPβCD on encapsulation efficacy during CUR:HPβCD inclusion complex (IC) formation using a solvent evaporation method. Qualitative and quantitative characterization performed on the CUR:HPβCD and CUR:HPβCD-loaded-BC hydrogels to assess their potential wound management applications is also discussed. As

far as the authors are aware, there are no studies reported in the literature on the production and characterization of CUR:HPβCD-loaded biosynthetic BC hydrogels for wound management applications.

2. Materials and Methods

2.1. Microorganisms, media and materials

Gluconoacetobacter xylinus (ATCC 23770) and *Staphylococcus aureus* (NCIMB 6571) were obtained from the University of Wolverhampton culture collection. Both microorganisms were maintained at -20 °C in a lyophilised form. Stock culture of *G. xylinus* was resuscitated on sterile mannitol agar (composition: yeast extract (5 g/L), peptone (3 g/L), mannitol (25 g/L), agar (15 g/L); all materials were purchased from Lab M, Bury, UK) and incubated for 48 h at 30 °C. Stock cultures of *S. aureus* were resuscitated on sterile tryptone soy agar (TSA) (Sigma-Aldrich, UK), prepared according to the manufacturer's protocol and sterilised by autoclaving prior to use, and incubated for 48 h at 37 °C. Overnight broth cultures were aseptically prepared in suitable broth using the stock plates prior to experimental use. Bacteriological peptone, yeast extract and dextrose for the Hestrin and Schramm (HS) culture media were purchased from Lab M (UK). HS medium was prepared following the standard protocol [20]. Tryptone soya broth (TSB), disodium phosphate and citric acid were purchased from Sigma-Aldrich (UK).

A549 lung adenocarcinoma, U251MG glioblastoma, MSTO mesothelioma and Panc 1 pancreatic ductal adenocarcinoma were purchased from ATCC (UK).

Hydroxypropyl-β-cyclodextrin (parenteral grade) was obtained from Roquette (France) and curcumin was purchased from Alfa Aesar (UK). Acetone was purchased from Fischer Scientific (UK). D_2O was purchased from Goss Scientific (UK). Ringer solution (1/4 strength) tablets were purchased from Lab M (UK) and prepared by dissolving one tablet in 500 mL of de-ionised water and sterilised prior to experimental use. Thiazolyl Blue Tetrazolium Bromide (MTT), sodium bicarbonate and 2,2-diphenyl-1-picrylhydrazyl (DPPH) were purchased from Sigma-Aldrich (UK). Dimethyl sulfoxide (DMSO), spectrophotometric grade, was purchased from Alfa Aesar (UK). Sodium hydroxide was purchased from Acros Organics (UK). NaCl (5.8 g/L) and glycine (7.6 g/L) were used for preparing Sorensen's glycine buffer and purchased from Sigma-Aldrich, UK. Trypsin was purchased from Lonza (Belgium). Dulbecco's Modified Eagle's Medium (DMEM), Fetal Bovine Serum (FBS), L-Glutamine and Antibiotic Antimycotic (10,000 units/mL penicillin, 10,000 µg/mL streptomycin and 25 µg/mL amphotericin B) were purchased from Gibco (UK).

2.2. Preparation and characterisation of CUR:HPβCD inclusion complex

2.2.1. Preparation of CUR:HPβCD inclusion complex

Inclusion complex of CUR with HPβCD was synthesised by the solvent evaporation (SE) method at the molar ratio of 1:1, following the protocol report by Yallapu, Jaggi, & Chauhan, (2010) [18], with appropriate modifications. In the current study, an attempt was made to prepare CUR:HPβCD inclusion complex by varying the volume ratio of solvents and evaluating the effect on encapsulation efficacy.

Briefly, CUR (0.79 g) was dissolved in acetone (5 mL) and HPβCD (3.0 g) was dissolved in deionised water (45 mL). CUR solution was added dropwise to the aqueous HPβCD solution under constant stirring in a Schott bottle covered with aluminium foil. As the volume ratio of acetone to water was 10 %, this sample was designated as IC 10. Similarly, using the same amounts of material (CUR 0.79 g and 3.0 g HPβCD) while varying the solvent volume ration, IC 25 (CUR in 12.5 mL acetone and HPβCD in 37.5 mL water); IC 50 (CUR in 25 mL acetone: HPβCD in 25 mL water), IC 75 (CUR in 37.5 mL acetone: HPβCD in 12.5 mL water) and IC 90 (CUR in 45 mL acetone: HPβCD in 5 mL water) were prepared (Table. 1). Stirring was performed in a fume hood at room temperature for up to 72 h by replacing the lids of Schott bottles with perforated aluminium foil to allow acetone to slowly evaporate. Samples were then centrifuged at 3000 rpm for 10 min and the supernatant containing water soluble inclusion complex of CUR:HPβCD was collected. The resultant inclusion complex was filtered through a 0.45 µm filter (MILLEX® HA, Merck Millipore) to remove any free CUR. The aqueous solution of ICs were then frozen at -20 °C overnight and lyophilised to obtain solid powders which were stored in dark for further experimental use.

Table 1: Summary of the preparation of CUR:HPβCD inclusion complexes by varying the volume ratio of solvent.

Inclusion complex	Mass of CUR (g)	Mass of HPβCD (g)	Volume of acetone to dissolve CUR (mL)	Volume of water to dissolve HPβCD (mL)	Volume ratio of acetone to water (%)
IC 10	0.79	3.00	5.00	45.00	10
IC 25	0.79	3.00	12.50	37.50	25
IC 50	0.79	3.00	25.00	25.00	50
IC 75	0.79	3.00	37.50	12.50	75
IC 90	0.79	3.00	45.00	5.00	90

2.2.2. Characterisation of CUR:HPβCD inclusion complex

The formation of the inclusion complex was confirmed by testing its physicochemical properties. In addition to the studies presented in this section, further characterisations like morphological study by SEM, chemical characterisation by FTIR were undertaken which are presented in section 2.3.3.

2.2.2.1. Solubility study

CUR, HPβCD and CUR:HPβCD (10 mg each) were weighed and added to deionised water (10 mL) in separate universal tubes. These were stirred for 1 h at room temperature (22 °C) followed by filtration using 0.45 µm filter. An aliquot was taken for UV-Visible spectrophotometric scan between 350-650 nm.

2.2.2.2. Determination of curcumin content and Encapsulation Efficiency (EE)

CUR content in the inclusion complex was quantified by using UV-Visible spectroscopy at a wavelength of 430 nm. The wavelength of 430 nm is the λ_{max} of CUR without any interference absorbance from HPβCD [21]. CUR:HPβCD (1 mg) was dissolved in dimethyl sulfoxide (DMSO) (5 mL) and gently shaken in an orbital shaker at 150 rpm at 37 °C for 1 h to extract CUR. The solution was filtered through 0.45 µm filter and CUR content was determined by UV-Visible spectroscopy at 430 nm. A standard calibration plot of CUR in DMSO was produced as a reference. The Encapsulation Efficiency (%) was determined using the formula:

$$\%\, EE = \frac{mass\ of\ encapsulated\ curcumin}{mass\ of\ curcumin\ initially\ used} \times 100$$

2.2.2.3. X-ray diffractometric analysis (XRD)

The X-ray diffraction patterns of CUR, HPβCD and CUR:HPβCD were obtained by an X-ray diffractometer (Empyrean, PANalytical, Neitherlands) with Cu radiation source. The X-ray diffractometer was set at a voltage of 40 kV and current of 40 mA.

2.2.2.4. Nuclear magnetic resonance (NMR)

The NMR experiments including ^{1}H, proton-decoupled ^{13}C, homonuclear correlation spectroscopy (COSY), heteronuclear single quantum correlation (HSQC), heteronuclear multiple bond correlation (HMBC), and rotating-frame nuclear Overhauser spectroscopy (ROESY) were performed on a 400 MHz JEOL NMR spectrometer JNM-ECZ400R/M1. The sample consisted of 10-20 mg of the inclusion complex dissolved in deuterium oxide. All spectra were internally referenced to residual solvent [22]. ^{1}H spectra were acquired with a 45° pulse and inter-pulse delay of 5 seconds across 16 transients with acquisition time of 2.18628 seconds and pulse width of 6.48 µs; ^{13}C NMR spectra were recorded with a 30° pulse and inter pulse delay of 5 seconds across 4097 transients with acquisition time of 1.03809 seconds, and pulse width of 10.338 µs; HSQC spectra were recorded using a matrix consisting of 256 × 819 points across eight scans with a relaxation delay of 3 seconds; HMBC spectra were recorded using a matrix consisting of 512 × 1638 points across eight scans with a relaxation delay of 3 seconds; COSY spectra were recorded by using a matrix of 1024 × 1024 points across 1 scan with a relaxation delay of 3 seconds; ROESY spectra were recorded in a phase sensitive mode with 1024 points in the *x* direction and 256 points in the *y* direction and acquired with 4 scans and relaxation delay of 1.5 seconds. Mixing time value was 0.25 seconds.

2.2.2.5. Thermal gravimetric analysis (TGA)

The evaluation of the thermal properties of CUR, HPβCD and CUR:HPβCD and physical mixture of CUR and HPβCD was undertaken using a Mettler Toledo Thermogravimetric Analyzer, TGA/DSC 1 STAR® System. Samples were subjected to TGA from 25 °C to 800 °C at 10 °C/min under constant flow of nitrogen (60 mL per minute). Differential thermogravimetry (DTG) curve was also studied as a first derivative of TGA curve.

2.2.2.6. Differential scanning calorimetry (DSC)

DSC scans of CUR, HPβCD, CUR:HPβCD and physical mixture of CUR and HPβCD were performed using DSC Q2000 (TA instruments, New Castle, DE). The scans were collected using

aluminum pans (TA instruments) with a nitrogen flow rate of 50 mL/min and temperature ramp rate of 20 °C/min.

2.3. Preparation and characterisation of CUR:HPβCD-loaded-BC hydrogels

2.3.1. Preparation of BC hydrogel pellicles

Bacterial cellulose (BC) hydrogel pellicles were prepared and purified by the protocol reported previously [7]. Briefly, *G. xylinus* was selected for biosynthesis of BC and grown in the Hestrin and Schramm (HS) culture medium under static condition by incubation at 30°C for 14 days. Biosynthesised pellicles were harvested after this period and purified by firstly boiling in 1% (w/v) aqueous sodium hydroxide and subsequently in deionised water until the BC became clear and transparent.

2.3.2. Loading CUR:HPβCD inclusion complex in BC hydrogel pellicles

It is important to note that due to the highest encapsulation efficacy, IC 75 was selected for loading and further characterisation. Purified BC pellicles were padded dry using filter paper and loaded with IC 75 by immersing in 2 % (w/v) aqueous solution of CUR:HPβCD overnight under constant agitation at 37 °C. Sterile conditions were maintained throughout the loading process.

2.3.3. Characterisation studies

CUR:HPβCD-loaded-BC hydrogels produced after loading the inclusion complex in padded dry BC were characterised to evaluate their properties for the potential wound dressing applications.

2.3.3.1. Scanning electron microscopy (SEM)

Solid samples of BC, CUR, HPβCD, CUR:HPβCD and lyophilised samples of CUR:HPβCD-loaded-BC were coated with gold using SC500 fine coater (Emscope, Kent, UK). The shape and morphology of these samples was studied using Zeiss Evo 50 EP, SEM (Carl Zeiss AG, Oberkochen, Germany).

2.3.3.2. Fourier transform infrared (FTIR) spectroscopy

FTIR of CUR, HPβCD, CUR:HPβCD and CUR:HPβCD-loaded-BC was recorded using a FTIR spectrophotometer (Bruker, Alpha, Platinum-ATR). The scanning range used was 400-4000 cm^{-1} with 16 scans settings for each sample run. A background scan was run prior to the scan of samples to obtain spectra.

2.3.3.3. Moisture content (M_c)

The wet mass (W_w) of BC (neat BC hydrogels) and BC hydrogel pellicles loaded with aqueous solution of CUR:HPβCD (2 % w/v) was determined before lyophilisation and the dry mass (W_d) was recorded after lyophilisation. M_C (%) was calculated using a formula:

$$\% M_c = \frac{(W_W - W_d)}{W_w} \times 100$$

2.3.3.4. Optical Transmission and Transparency test

The quantitative optical transmission (%) of hydrogels was determined using LI-250A Light meter (LI-COR® Biosciences). BC pellicles were padded dry and rehydrated either with deionised water (neat BC) or 2 % (w/v) aqueous solution of CUR:HPβCD (test hydrogels) and optical transmission (% T) of light was read. Readings were taken for petri dish with deionised water (control), neat BC pellicles in petri dish and test BC pellicles. Four readings from a different sections of each neat and test BC pellicles were recorded and averages used to examine the % T by comparison to the control (100 % T).

Moreover, the neat and 2 % CUR:HPβCD-loaded-BC hydrogels were transferred on the laminated paper with text in different colours. The clarity of letters beneath each hydrogel was examined to determine if it would permit observation and assessment simulating to wound monitoring context.

2.3.3.5. Water vapour transmission rate (WVTR)

The WVTR of neat BC and CUR:HPβCD-loaded-BC hydrogel dressings was measured using the cup test method according to the American Society for Testing and Materials (ASTM) standard [23,24]. In the current study, to achieve controlled conditions with minimum variations in set parameters during the entire length of the experiment, hypoxia incubator (Optronix, Oxford, UK) was used instead of saturated salt chamber as reported previously [25]. An incubator temperature of 35±0.1 °C and 60±1 % relative humidity [RH] was maintained using compressed air during the entire period of the experiment. There was no attempt to artificially adjust air flow in the chamber as the influence of local air velocity was not examined in this study. A digital balance (ON BALANCE^{TM}, Myco MZ-100-BK) was placed inside the chamber for weighing the assemblies. The selected temperature (35 °C) corresponds to the temperature of the wound site as reported by Lamke *et al*., 1977 [26].

Purified BC pellicles were padded dry and rehydrated either with deionised water (neat BC) or 2 % (w/v) CUR:HPβCD aqueous solution (test hydrogels) under agitated conditions at 150 rpm and 37 °C overnight in an orbital shaker. Thickness of the rehydrated BC pellicles was measured using a Vernier calliper (Whitworth Digital calliper). Four readings for each pellicle were taken and average thickness calculated. Neat BC and/or CUR:HPβCD-loaded-BC hydrogels (2.44 cm exposed diameter) were secured onto glass vessels containing 7.5 mL distilled water. The assemblies were kept in the chamber in upright position. WVTR was determined (in triplicates) by weighing the complete beaker assembly inside the chamber at set time intervals and calculated as [27]:

$$WVTR = \frac{slope \text{ x } 24}{test\ area\ in\ m^2}\ g/m^2/day$$

2.4. *In vitro* tests of CUR:HPβCD-loaded-BC hydrogels

2.4.1. Haemocompatibility

In the current study, with the intended wound management applications, the haemocompatibility of CUR:HPβCD-loaded-BC hydrogels was evaluated *in vitro,* by assessing haemolytic potential of hydrogels. The test was performed as previously reported for testing haemocompatibility of BC with some modifications [25]. Briefly, defibrinated horse whole blood (purchased from

TCS Biosciences Ltd) was washed with sterile 0.9 % saline (pH 5.5) twice and centrifuged at 3000 rpm for 10 min before re-suspending in saline solution. 2 % (w/v) CUR:HPβCD was prepared in saline and loaded in padded dry BC pellicles. Using the biopsy punch, CUR:HPβCD-loaded-BC discs (≈8.0 mm) were cut and incubated with 1.9 mL saline-suspended horse blood cells in test Eppendorfs under sterile conditions. Positive (+ve) controls were distilled water suspended blood cells and negative (-ve) controls were blood cells suspended in saline. Eppendorfs were incubated at 4 °C for 2 h with gentle inversion after every 15 min. Post-incubation, BC discs were removed under sterile condition followed by each sample being centrifuged at 3000 rpm for 10 min and supernatant decanted. Absorbance was recorded at 540 nm and percentage (%) haemolysis was determined as follows:

$$\%\ Haemolysis = \frac{(Abs\ of\ sample) - (Abs\ of\ -ve\ control)}{(Abs\ of\ +ve\ control) - (Abs\ of\ -ve\ control)} \times 100$$

2.4.2. Cytocompatibility (*in vitro* cell viability)

Cytocompatible nature of BC has been previously reported [25]. To study the effect of the CUR:HPβCD-loaded-BC on cell viability, the previously reported study was extended on 4 human cancer cell lines from different tissues, namely, A549 (human lung adenocarcinoma), MSTO (human mesothelioma), PANC1 (human pancreatic ductal adenocarcinoma) and U251MG (human glioblastoma).

All cell lines were cultured in DMEM medium containing 4.5 g/L glucose, supplemented with fetal bovine serum (10 %), Antibiotic Antimycotic (1 %), L-Glutamine (2 mM) and incubated at 37 °C in a humidity incubator with 5 % CO_2. The cytocompatibility of free CUR:HPβCD and CUR:HPβCD-loaded-BC was investigated. Four different concentrations of CUR:HPβCD (1 %, 1.25 %, 1.5 %, 2 % w/v) were prepared in Dulbecco's Modified Eagle's Medium (DMEM). BC pellicles were padded dried and either rehydrated with DMEM (control) or the respective concentrations of CUR:HPβCD in DMEM (test) in an orbital shaker at 37 °C at 150 rpm for overnight. Discs (≈8.0 mm diameter) were cut from the control and test pellicles using a corer for the experimental purposes. The whole procedure was conducted aseptically.

Briefly, 25,000 cells per well were seeded in 24 well plates for 24 h at 37 °C in 5% CO_2 incubator. The cells were then exposed to either free CUR:HPβCD or CUR:HPβCD-loaded-BC discs for 24 h. After incubation, the morphology of cells, confluence of the cell monolayer and cell viability was observed microscopically using an inverted light microscope (Nikon, Japan). The effect

of free CUR:HPβCD and CUR:HPβCD-loaded-BC discs on cell viability was evaluated by standard MTT cytotoxicity assay by adding 5 mg/ml MTT solution (Sigma, UK) in all the wells and incubated for 2 h, followed by solubilising the formazan crystals with DMSO and Sorensen's glycine buffer (pH 10.5). All experiments were done in triplicates and cell viability was calculated using the mean absorbance measured at 540 nm and the results were statistically analysed by two-way ANOVA with a Tukey's multi comparisons test using GraphPad Prism.

2.4.3. Curcumin release study

Small (≈8.0 mm diameter) sized discs of purified BC were cut using a biopsy punch and padded dry on filter paper. These discs were loaded with 2 % (w/v) aqueous solution of CUR:HPβCD by incubating overnight at 37 °C in glass Bijoux bottles, under agitated conditions at 150 rpm.

These discs were transferred to individual Bijoux tube containing 1 mL 0.9 % saline (pH 5.5) and incubated under static conditions at 35 °C. At set intervals, discs were moved to a new set of bijoux tubes with fresh 1 mL saline and incubated under same conditions. This was repeated over 48 h and CUR release was spectroscopically assessed at 430 nm for each time interval.

The standard calibration curve of CUR in 0.9 % saline (pH 5.5) was produced as a reference. Briefly, the stock solution (1000 µg/mL) of CUR was prepared by taking CUR (10 mg) and dissolving in ethanol:saline (70:30 % v/v) and making up to 10 mL. A standard solution (30 µg/mL) was prepared by taking 150 µL of stock solution and making up to 5.0 mL using saline. Using this standard solution, other standards were prepared in saline and the standards were read at 430 nm using saline as blank.

2.4.4. Antimicrobial activity by disc diffusion assay:

The antimicrobial activity of BC loaded with 2 % (w/v) aqueous CUR:HPβCD was investigated against *S. aureus*, using the disc diffusion assay; purified BC and BC loaded with HPβCD were used as controls. Discs of BC, BC-HPβCD and BC-CUR:HPβCD (≈8.0 mm diameter) were aseptically cut and placed on TSA plates spread with overnight culture of *S. aureus* and following incubation at 37 °C for 24 h, the zone of inhibition (ZOI) was measured. Results are presented for ZOI (mm) at 24 h and analysed by one-way ANOVA with a Tukey's multi comparisons test using GraphPad Prism.

2.4.5. Anti-oxidant activity by DPPH assay

2,2-diphenyl-1-picrylhydrazyl (DPPH) radical scavenging assay was performed according the protocol reported by [28] with appropriate modification. Briefly, test solutions of varying concentrations of CUR:HPβCD in methanol were prepared and methanol was used in preparing a blank. The assay mixture with 1 mL DPPH (80 µg/mL) methanolic solution and 1 mL solutions of various concentrations of the material (including a blank) after mixing were incubated in dark for 30 min at room temperature. Absorbance was measured spectrophotometrically at 517 nm. The free radical scavenging capacity was calculated as percent antioxidant effect (% E) using the following equation. Different sample concentrations were used to produce a curve for calculating IC_{50} values, the amount of sample required to obtain 50 % of the free radical inhibition [29].

$$\%E = \frac{Abs_{control} - Abs_{sample}}{Abs_{control}} \times 100$$

3. Results and discussion

3.1. Preparation of CUR:HPβCD-loaded-BC hydrogels

G. xylinus produced BC hydrogel pellicles in 2 weeks under static conditions. These pellicles were harvested and purified to get rid of entrapped bacterial cells and excess media. The hydrogel pellicles after purification became clear and transparent (Fig. 1a) which is in accordance with our previous study [7]. The BC pellicles after purification were ready for loading with CUR:HPβCD.

CUR:HPβCD (yellow powder) was produced from the CUR (dark yellow powder) and HPβCD (white powder) by solvent extraction method which is in accordance with the literature [18]. The novel approach taken in this study to produce IC 10, IC 25, IC 50, IC 75 and IC 90, supramolecular inclusion complexes revealed that varied solvent volume ratios have an influence on CUR content encapsulated in HPβCD. The EE (%) results of IC 10, IC 25, IC 50, IC 75 and IC 90 revealed 3.64±0.16 %, 3.84±0.37 %, 7.37±1.24 %, 18.26±1.02 % and 16.34±0.75 % (n=3) encapsulation efficacy respectively. These results suggested that IC 75 produced by CUR dissolved in 37.5 mL acetone and HPβCD dissolved in 12.5 mL water for the inclusion complex production gave highest % EE hence it was selected as a standard procedure for the preparation of inclusion complex for further experimental investigations. It is important to note that all the characterisations for CUR:HPβCD were done using IC 75. CUR content determined in IC 75 samples was in the range of 3.28±0.38 % (n=4).

IC 75 was loaded in padded dry BC to produce hydrogels for wound management applications. Visual inspection of purified BC hydrogel pellicles loaded with 2 % (w/v) CUR:HPβCD revealed highly consistent loading (Fig. 1b). After loading of the inclusion complex, the colour of BC hydrogels changed from clear to orange yellow (Fig. 1a-b).

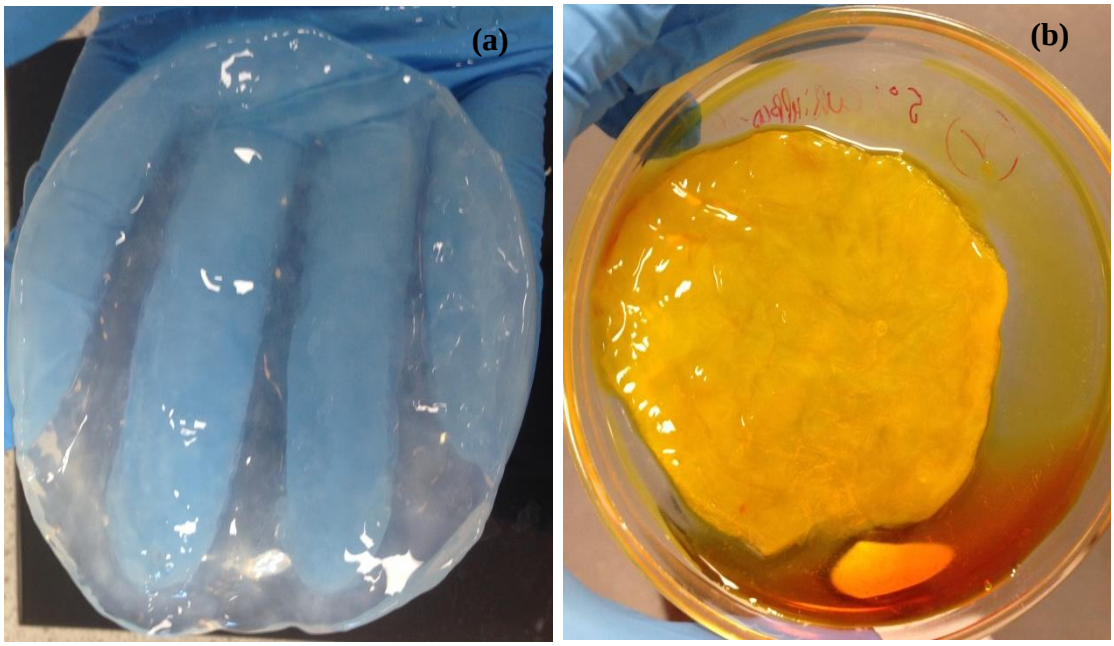

Figure 1: Visual appearance of **(a)** BC hydrogel pellicle after purification **(b)** CUR:HPβCD-loaded-BC hydrogel pellicle.

3.2. Characterisation studies of CUR:HPβCD inclusion complex and CUR:HPβCD-loaded-BC hydrogels

3.2.1. Solubility in water: CUR versus CUR:HPβCD inclusion complex

CUR exhibits the maximum absorbance at ≈430 nm [30]. In the current study, the inclusion of CUR in HPβCD enhanced its aqueous solubility which was evident in the spectral scan (Fig. 2). The UV-Visible spectrum of aqueous filtrate of CUR didn't exhibit significant absorption in the specified spectral range suggesting low aqueous solubility of CUR at the aforesaid conditions. Moreover, the aqueous solution of HPβCD didn't show significant absorbance in the selected range. In case of the CUR:HPβCD, there was strong absorbance recorded around 430 nm due to enhanced aqueous solubility of CUR. These results correspond with previous studies that CUR has poor aqueous solubility which could be enhanced by its inclusion in CD cavity [19,31,32].

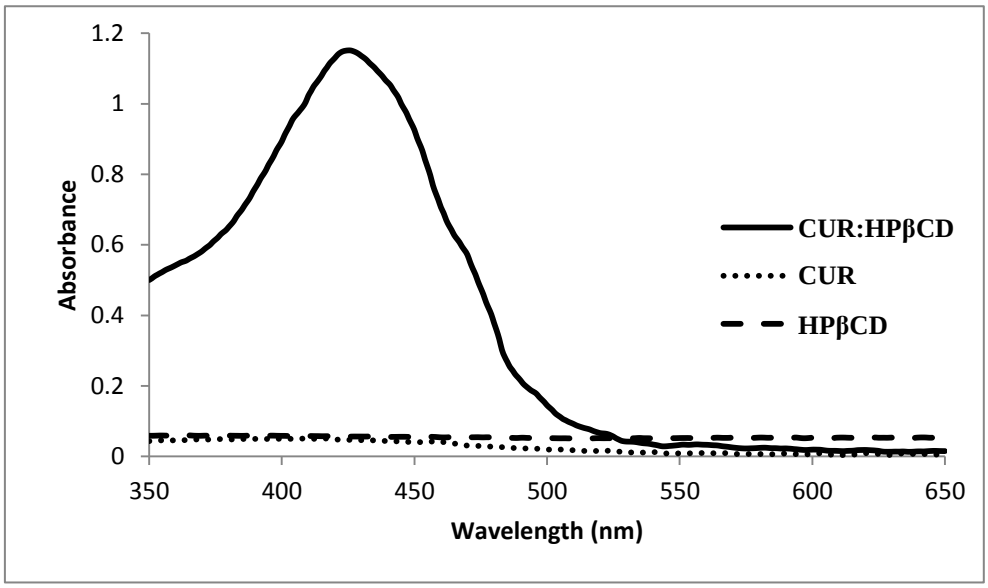

Figure 2: UV-Visible absorption spectra of CUR, HPβCD and CUR:HPβCD dissolved in water after 1 h stirring at room temperature followed by filtration through 0.45 µm filter.

3.2.2. X-ray Diffractometric analysis (XRD)

The XRD spectra of CUR, HPβCD and lyophilised CUR:HPβCD are shown in Fig. 3. Results revealed that CUR exists in a crystalline form which is indicated by the characteristic peaks (Fig. 3a) whereas HPβCD is amorphous (Fig. 3b) in nature. After complexation with HPβCD, there was no noticeable evidence of crystallinity of CUR in the inclusion complex (Fig. 3c). This suggests that CUR may have formed an inclusion complex with HPβCD leading to the loss of peaks. These results are in accordance with literature findings [19,33,34].

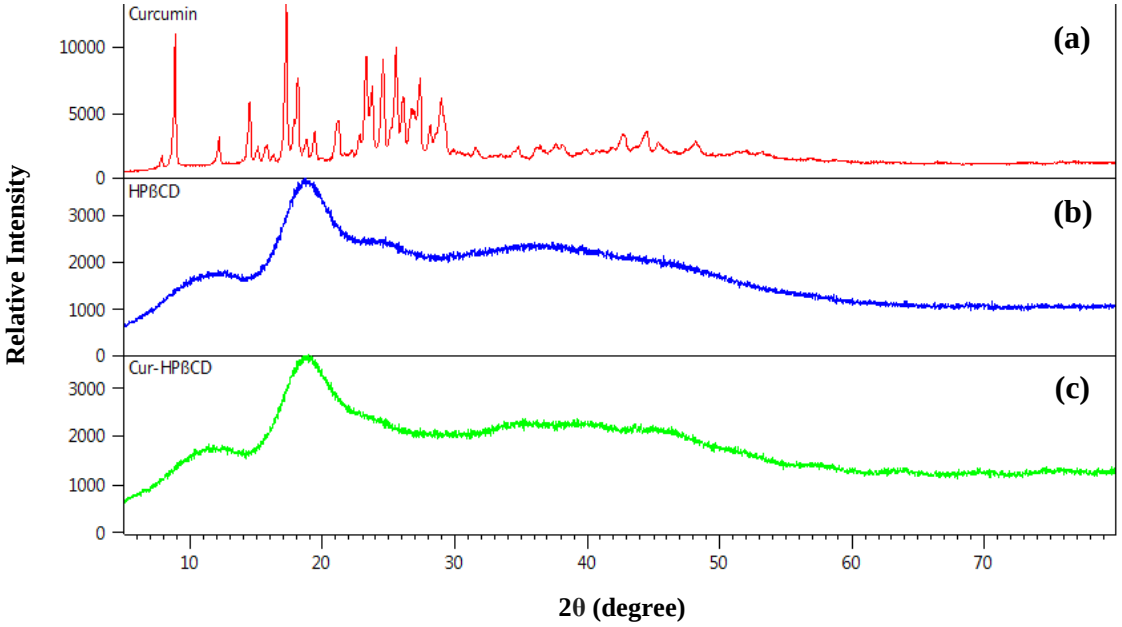

Figure 3: XRD results of **(a)** CUR **(b)** HPβCD **(c)** CUR:HPβCD.

3.2.3. Nuclear Magnetic Resonance spectroscopy (NMR)

NMR spectroscopy was used to investigate the success of the formation of the inclusion complex between hydroxypropyl-β-cyclodextrin and curcumin (sample IC 75). The ^{1}H and ^{13}C NMR data of the CUR:HPβCD was assigned using a combination of previously reported proton NMR data [35] and 2D NMR techniques (COSY, HSQC and HMBC) (see ^{1}H and ^{13}C NMR data in Fig. S2-S5 in the supporting information).

Evidence for the formation of the CUR:HPβCD inclusion complex can be chiefly observed through both ^{1}H and ROESY NMR. Upon inspection of the ^{1}H NMR spectra, CUR:HPβCD displayed a distinctive upfield shift in the proton resonances of the internally facing protons (ca. 0.01 ppm), H^{3} and H^{5} of HPβCD upon inclusion of CUR in comparison to the neat HPβCD; the

resonances of the externally facing protons of CUR:HPβCD remained unchanged (Fig. S6 and S7; see Scheme S1a-c for structural assignments in the supporting information). This indicates a change in the local magnetic environment of the HCβCD protons in the presence of the CUR aryl/alkenyl group(s).

Further conclusive evidence for the formation of CUR:HPβCD was subsequently obtained by ROESY NMR analysis; a ROESY correlation between H^5 of HPβCD and CUR aryl protons spectrum clearly indicates the space interaction indicative of an inclusion complex (Fig. 4).

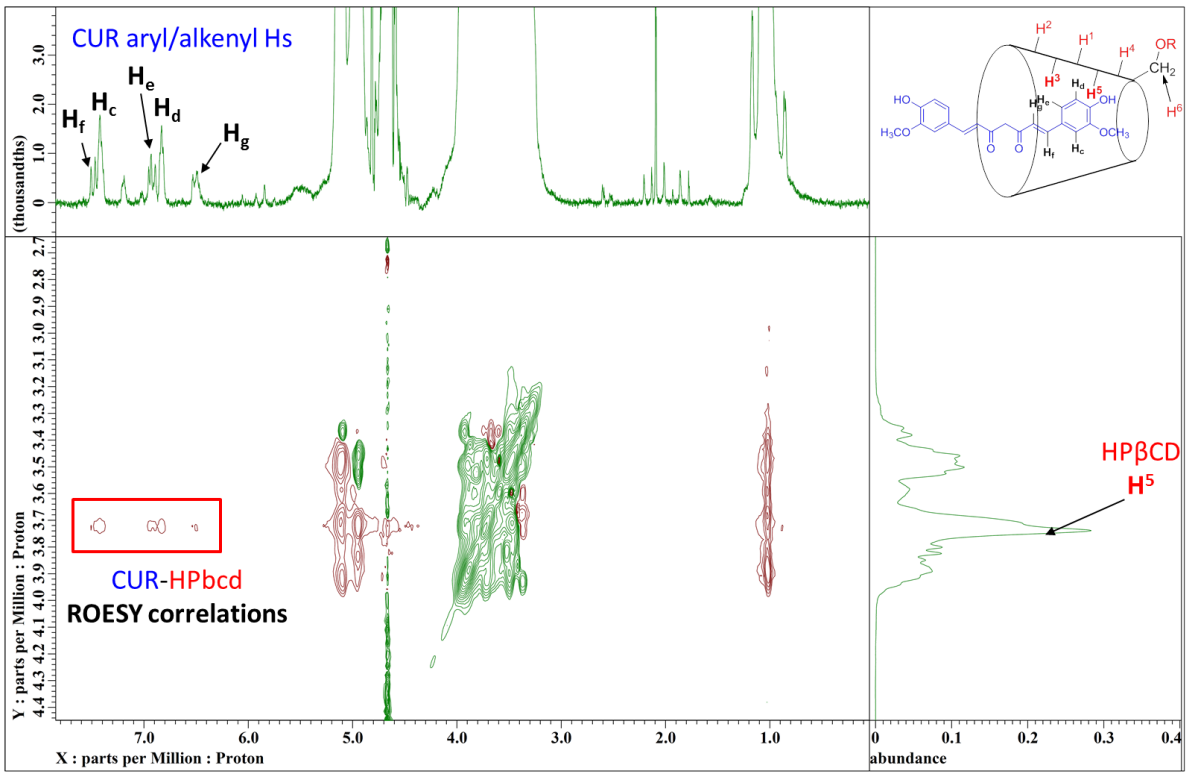

Figure 4: Expansion of the ROESY spectrum of the CUR:HPβCD inclusion complex in D_2O indicating correlation cross peaks between HPβCD and CUR (inset: schematic structure of the inclusion complex).

3.2.4. Thermal Analysis (TGA and DSC)

The thermal analytical techniques like TGA and DSC are widely used in pre-formulation studies. The thermokinetic data could be used to understand the thermal decomposition reaction and helps determine the storage conditions. Moreover, the comparison of TG curves of pure compounds, their physical

mixture and the CUR:HPβCD inclusion complex could provide evidence of interactions between compounds and the formation of inclusion complex [36].

Thermal behaviour of CUR, HPβCD, CUR:HPβCD was investigated and compared to CUR and HPβCD physical mixture, to understand the solid-state characterisation and thermal stability of the inclusion complex during production and storage. Thermogravimetric data revealed that thermal degradation of CUR starts at around 220 °C, which is ≈ 40 °C above its melting point. It loses around 54 % mass between 300-420 °C. HPβCD mass loss of nearly 6 % at around 91 °C attributed to the loss of water and major mass loss (>70 %) peaks at 344 °C due to the decomposition of the molecule (Fig. 5a-b). These weight losses were visible in both, the physical mixture and CUR:HPβCD inclusion complex. On further examination, it was noticed that the inclusion complex displayed higher thermal stability as shown in Fig. 5a-b but as our study aims at the application of the product at the physiological temperature so the decomposition at high temperatures (>300 °C) was not significant. It should be noted that due to the inclusion of CUR in HPβCD cavity, the thermal behaviour of CUR was different from free CUR which is in accordance with literature [36].

The thermokinetic data did not show decomposition at normal working temperatures suggesting that the production and storage of the inclusion complex at room temperature does not affect its thermal stability. BC is thermally stable at the standard autoclaving temperatures [25]. The data from the current study suggests that the inclusion complex is also thermally stable at such temperatures. Since BC and the inclusion complex are both thermally stable at the standard autoclaving temperatures, the hydrogel dressings may be sterilised by autoclaving prior to the application on the wound site.

DSC analysis was performed to further corroborate the results obtained from TGA. DSC results of CUR revealed an enthalpy change with a sharp endotherm in the region of 179 °C indicative of its melting point (Fig. 5c). In the case of HPβCD, there was observed two endotherms around 259 °C and 291 °C followed by its decomposition (Fig. 5c). In the case of physical mixture, the characteristic endotherms of CUR appeared at 179 °C suggesting free CUR in the physical mixture. Moreover, endotherm peaks attributed to HPβCD were also visible. However, shift in peak positions was observed (Fig. 5c) which could be due to the interactive effect of HPβCD with CUR on mixing, which is in accordance with literature findings [19]. The thermogram of CUR:HPβCD revealed that the melting endotherm peak for CUR in the inclusion complex disappeared, suggesting that CUR was protected up to 244 °C. Moreover, the shift in endotherm peaks attributed to HPβCD in CUR:HPβCD inclusion complex was observed. This may be due to molecular

556 interactions of inclusion of CUR in the HPβCD cavity (Fig. 5c) thus indicating
557 the formation of the inclusion complex.

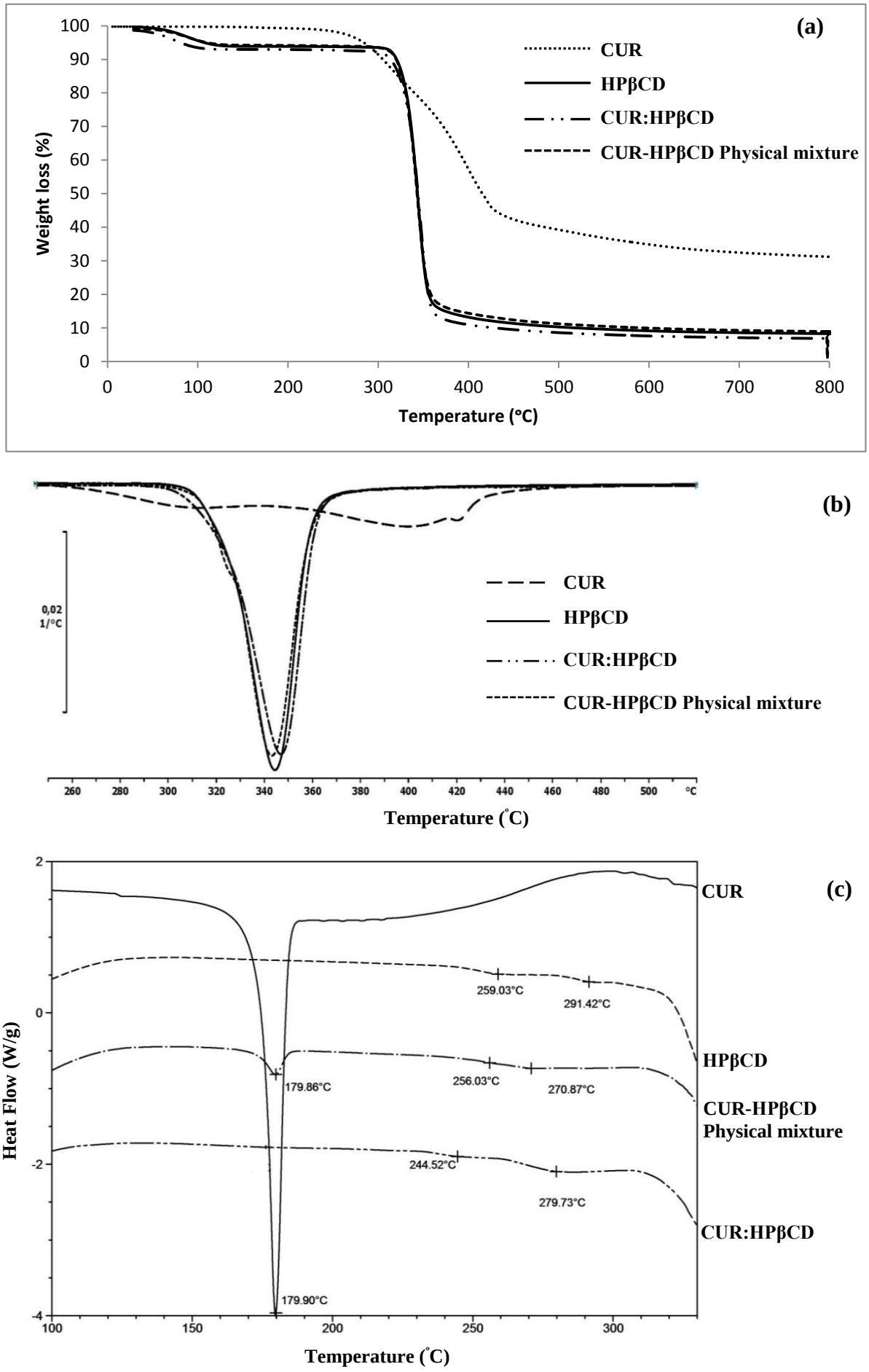

Figure 5: (a) TGA curves **(b)** DTG curves **(c)** DSC spectra of CUR, HPβCD, CUR, HPβCD Physical mixture and CUR:HPβCD.

558

3.2.5. Scanning electron microscopy (SEM)

BC appears as a dense interwoven fibre network [7]. It emerged that the fine ribbons (30-105 nm thickness) (Fig. 6a) of cellulose entangle with each other forming the network structure interspersed with voids. Morphological studies of lyophilised purified BC revealed two types of pores in the BC network structure; nano pores with pore size as low as 27 nm (Fig. 6b) and some large superficial pores with diameter value of up to 10 μm (Fig. 6c). It may be noted that these pores may further expand on hydration with water. SEM results revealed that the shape of CUR and HPβCD changed from round to irregular shape to plate like structures in CUR:HPβCD (Fig. 6d-f). When padded dry BC was rehydrated by immersion in aqueous solution of CUR:HPβCD, the voids allowed penetration of the inclusion complex which then got physically entrapped in the BC fibre network (Fig. 6g). This resulted in the production of CUR:HPβCD-loaded-BC hydrogels.

575

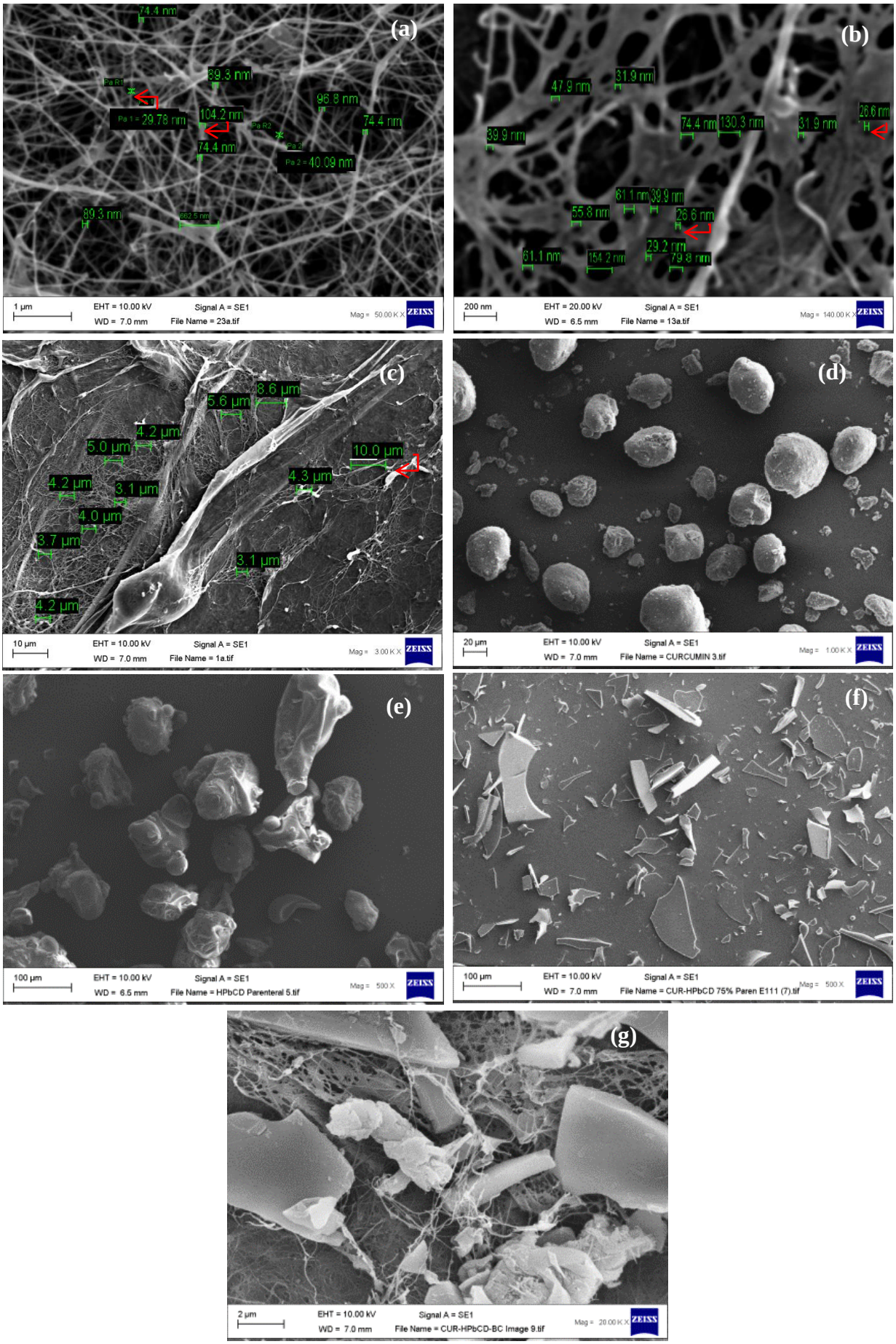

Figure 6: SEM images of **(a - c)** BC morphology with fibre thickness and pore size distribution **(d)** CUR **(e)** HPβCD **(f)** CUR:HPβCD **(g)** CUR:HPβCD-loaded in BC.

3.2.6. Fourier transform infrared (FTIR)

A detailed investigation on the vibrational spectra of CUR, HPβCD and BC has been reported in literature [7,19,32]. FTIR spectral results of CUR, HPβCD, CUR:HPβCD, purified BC and CUR:HPβCD-loaded-BC are illustrated in Fig. 7. The characteristic sharp peak at 3504 cm^{-1} and a broad peak at band regions of 3308 cm^{-1} suggested the presence of OH; 1619 cm^{-1} was assigned to C=C and C=O vibrations; 1591 cm^{-1} to the stretching vibrations of benzene ring and 1497 cm^{-1} to the C=C (Fig. 7a). For HPβCD the characteristic broad peak at 3340 cm^{-1} was assigned to stretching vibrations of OH group; 2927 cm^{-1} to C-H stretching and other prominent peaks presented at 1156 cm^{-1} and 1084 cm^{-1} (C-H), 1024 cm^{-1} (C-O-C glucose units) (Fig. 7b). In CUR:HPβCD, due to the encapsulation of CUR in HPβCD cavity, the peaks of CUR appeared to be masked or shifted. The prominent peaks at 3504 cm^{-1} and 1619 cm^{-1} appeared to be masked by HPβCD molecular vibrations in the inclusion complex (Fig. 7c) which could be due to the inclusion of CUR in HPβCD cavity [19,31,32].

BC has characteristic peaks at 3342 cm^{-1}, 2899 cm^{-1}, 1640 cm^{-1}, 1370 cm^{-1}, 1159 cm^{-1}, 1057 cm^{-1} (Fig. 7d). These peaks appeared in CUR-HPβCD-loaded-BC spectra (Fig. 7e). Furthermore, the characteristic peaks of the inclusion complex were also observed in the spectra (Fig. 7e), thereby confirming the loading of the inclusion complex in the BC network.

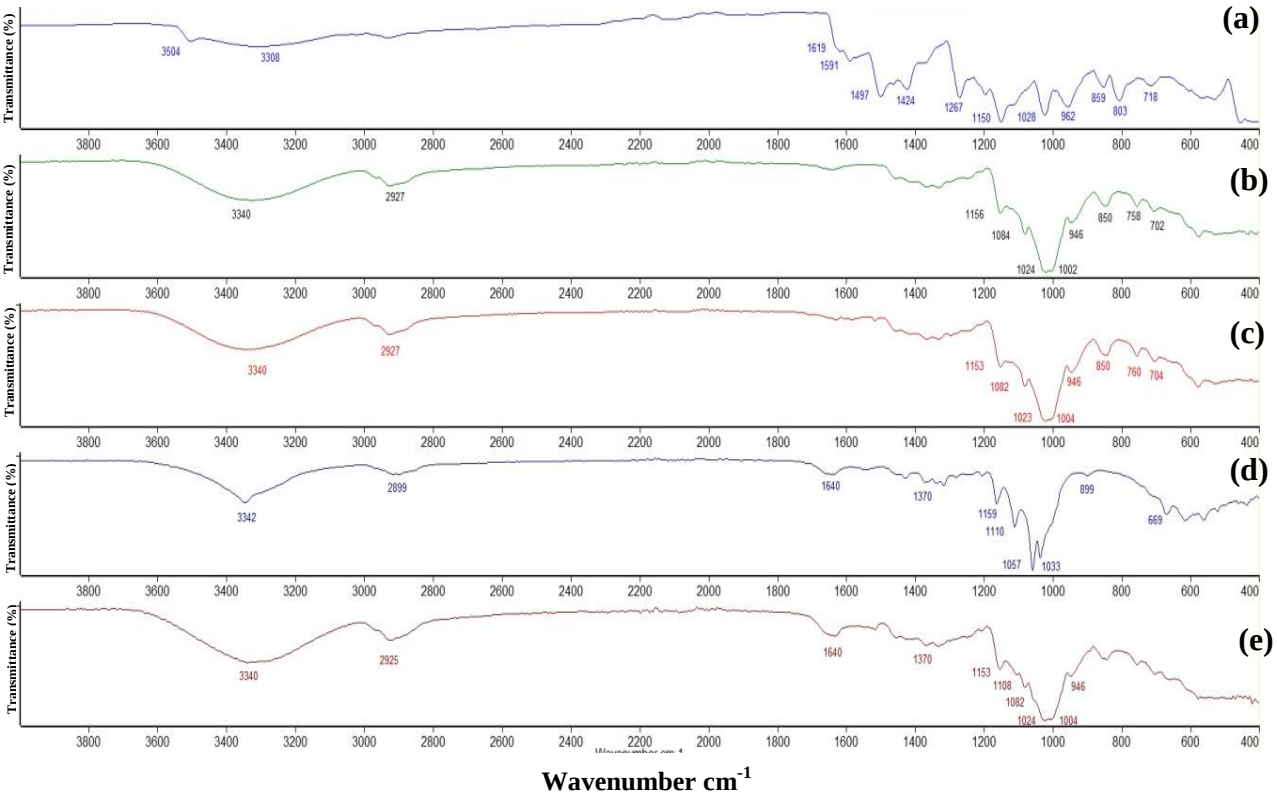

Figure 7: FTIR spectra from 400-4000cm^{-1} for **(a)** CUR **(b)** HPβCD **(c)** CUR:HPβCD **(d)** bacterial cellulose **(e)** CUR:HPβCD-loaded-BC.

3.2.7. Moisture content (M_c)

BC hydrogels have high water content and the results of the moisture content determination study revealed neat BC hydrogels imbibed >99.5 % (n=4) water which is accordance with previously published data [25]. Moreover, the results revealed that BC loaded with 2 % (w/v) CUR:HPβCD imbibed 97.63±0.057 % (n=4) water. These results suggested that CUR:HPβCD inclusion complex that gets physically trapped in BC fibres (as suggested in Fig. 6g) contributes to this difference between neat BC and CUR:HPβCD-loaded-BC.

Wound dressings with high moisture content offers several benefits including, but not limited to, high malleability, easy and pain free removal of the dressing, cooling and soothing effect resulting in a sensation of pain reduction with a capability of developing a moist microclimate that has been proven to enhance epithelialisation [1,3,5,37,38]. The high moisture content in CUR:HPβCD-loaded-BC hydrogels produced in the current study would deliver these beneficial attributes and contributes towards facilitating wound healing along with patient comfort and compliance.

3.2.8. Optical Transmission and Transparency test

The appearance of the wound site is vital to assess patients' response to the treatment. A basic technique to carry out this assessment is by visual observation of the wound site by the removal of the dressing, however removal of the dressing from the wound site could cause trauma [3]. Non-invasive monitoring of the healing process without the need to remove the wound dressing has the potential to ensure effective management [39]. This would allow regular clinical assessment of the wound healing process, improve patient comfort and potentially lower the cost of treatment with less frequent dressing change.

Transparency is a property that measures the ability of the material to allow the light pass through without scattering [40]. In the current study an attempt was made to produce the hydrogel dressings delivering this feature. Neat BC hydrogels demonstrated the % Transmission of 85.72±1.57 % (n=3). Although, the light transmittance of CUR:HPβCD-loaded-BC hydrogel dressings was reduced, this is sufficiently high (66.13±2.36 %) (n=3).

On further evaluation, the clarity of letters through the hydrogels supported high transparency through both the neat and CUR:HPβCD-loaded-BC hydrogels (Fig. 8). These results support the capability of CUR:HPβCD-loaded-BC hydrogel dressings for non-invasive clinical wound monitoring.

Several protocols have been reported in the literature to evaluate the transparency of hydrogels with wound dressing applications [37,41]. The authors are mindful that the method designed and employed in the current study for transparency testing may not exactly mirror the real wound site; for that to be considered, this study could be extended to *in vivo* animal models. Nevertheless, this method has several advantages due to its simplicity and low cost.

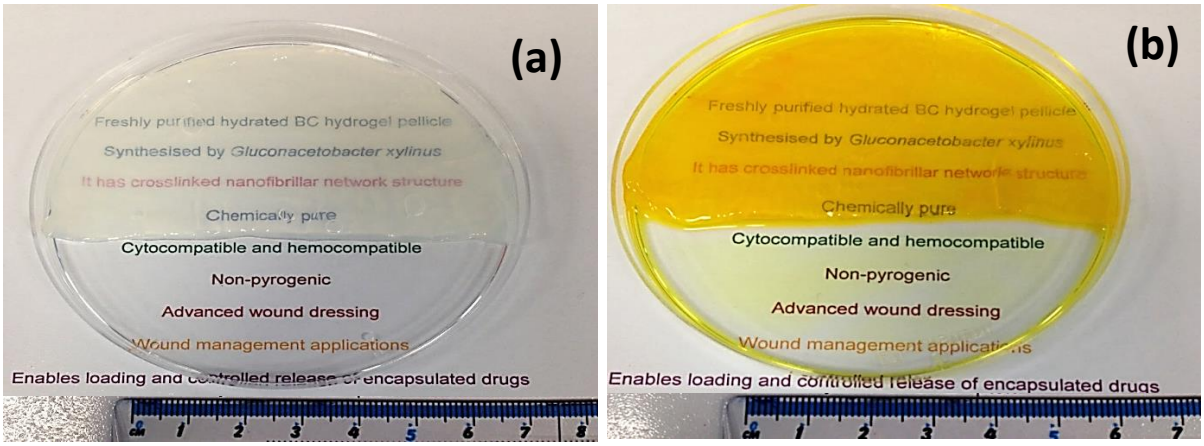

Figure 8: Visual appearance of text through **(a)** neat BC sheet **(b)** 2% CUR:HPβCD-loaded-BC.

3.2.9. Water Vapour Transmission Rate (WVTR)

Normal skin has the ability to control the water loss by evaporation from the body, to prevent dehydration, which gets compromised when the integrity of the skin is affected by injury. Lamke, Nilsson, & Reithner, 1977 [26] reported the evaporation water loss of 204±12 g/m^2/24 h from the normal skin which could go up to 5138.4±201.6 g/m^2/24 h in case of a granulating wound.

An ideal wound dressing material must have a property to control the evaporative water loss from the wound [24]. High WVTR may lead to dehydration and scab formation whereas very low WVTR may lead to the accumulation of exudate, maceration of periwound skin and increased risk of infections [38].

In the current study, WVTR was evaluated as the gradient of weight loss from the samples versus time. The thickness of rehydrated hydrogels (neat and test) was in the range of 1.5-2.5 mm. WVTR values for neat BC were in the range of 2526.32-3137.68 g/m^2/24 h (n=3) and for 2 % CUR:HPβCD-loaded-BC were 2258.53-2460.63 g/m^2/24 h (n=3). Previous reported studies suggest that a WVTR level of 2000-2500 g/m^2/24 h would be sufficient to maintain an optimum moist environment at the wound site [24,25,42]. Our results revealed that the WVTR range of CUR:HPβCD-loaded-BC hydrogels were close to the

recommended range hence would be suitable for wound healing applications. Moreover, the results revealed that the loss of water from neat BC hydrogels was more than from the test hydrogels (CUR:HPβCD-loaded-BC). We postulated this is due to the CUR-HPβCD loaded in the BC network structure reducing the void space in the hydrogels and controlling the transmission of water in CUR:HPβCD-loaded-BC hydrogels compared to neat BC.

3.3. *In vitro* characterisation of CUR:HPβCD-loaded-BC hydrogels

3.3.1. Biocompatibility studies (Haemocompatibility and Cytocompatibility)

When materials come in contact with blood, they may cause haemolysis of the blood cells thus assessment of haemolytic properties become vital for materials with potential biomedical applications. According to the ASTM F756 standards [43], haemolytic indices, the test samples can be: (a) haemolytic materials with haemolysis >5 % (b) slightly haemolytic with haemolysis between 2-5 % and (c) non-haemolytic materials having haemolysis below 2 % [44]. The *in vitro* blood compatibility results revealed that the test hydrogels are haemocompatible with % haemolysis <0.20 % (n=9) which is well below the acceptable limit for haemolysis. These results confirmed that CUR:HPβCD-loaded-BC hydrogels are non-haemolytic material and suitable for wound management applications.

BC has been reported to be cytocompatible for biomedical applications [25,37]. Cytocompability is one of the many properties of BC leading to its use in fabricating proprietary wound dressings. High bacterial burden at the wound site has deleterious effect on the wound healing hence the use of antimicrobial becomes imperative. Since bacteriostatic and/or bactericidal agents may have harmful effect on the host cells, therefore a benefit:risk ratio has to be evaluated for the selection of antimicrobial wound dressings [45]. The use of proprietary silver dressings in chronic wound management to control the microbial bioburden is a good example where the benefit outweighs the risk of cytotoxic effect of silver [45,46]. In the current study, the MTT cytocompatibility study aims to find out how the CUR released from the hydrogels affects the survival of mammalian cells. The cytotoxicity as determined by MTT assay demonstrated that the CUR:HPβCD-loaded-BC hydrogels has varied compatible with the tested cell lines (Fig. 9a). Despite the varied response, all cell lines demonstrated cell viability when exposed to CUR:HPβCD or CUR:HPβCD-loaded-BC hydrogels (Fig. 9a-c). Four different cell lines were used in this study and most of them tolerated up to 2% CUR:HPβCD over 24hrs and showed very good survival rates. Despite being very sensitive, the A549 cell line also showed around 60 % survival at the highest tested dose (2 %). Although this will be a significant decrease in cell

699 survival in comparison to control, this dose has not even reached the standard
700 IC50/50% cell death to define this as a highly toxic effect. Moreover, in
701 patients, this will correspond to how much free CUR is being released from
702 the material and get in the systemic circulation. It is very unlikely that this
703 amount will cause the toxic effect to vital organs.
704
705 Furthermore, we compared the cytocompatibility of CUR:HPβCD-loaded-BC
706 hydrogels with that of free CUR:HPβCD (equivalent amount). The results
707 showed that there was no significant difference ($p>0.05$) between the free
708 CUR:HPβCD or the 2 % CUR:HPβCD-loaded-BC hydrogels. This indicated
709 that the BC matrix used to deliver CUR:HPβCD inclusion complex does not
710 affect the cell viability.

711 Our results are in accordance with other cytotoxicity studies reporting the
712 cytocompatible nature of CUR and its conjugates for biomedical applications
713 [47-49]. These findings further support the potential wound dressing
714 applications of CUR:HPβCD-loaded-BC hydrogels.

715

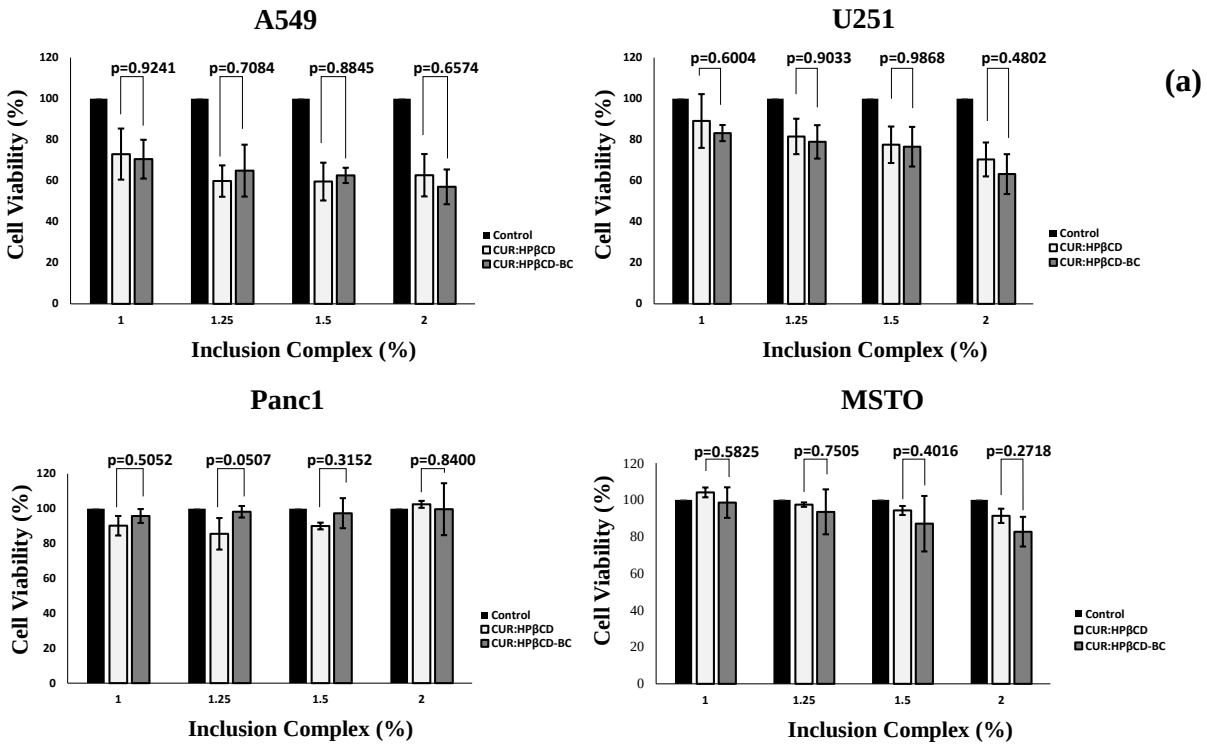
A549
U251
Panc1
MSTO
Cell Viability (%)
Inclusion Complex (%)
Control
CUR:HPβCD
CUR:HPβCD-BC
p=0.9241
p=0.7084
p=0.8845
p=0.6574
p=0.6004
p=0.9033
p=0.9868
p=0.4802
p=0.5052
p=0.0507
p=0.3152
p=0.8400
p=0.5825
p=0.7505
p=0.4016
p=0.2718
(a)

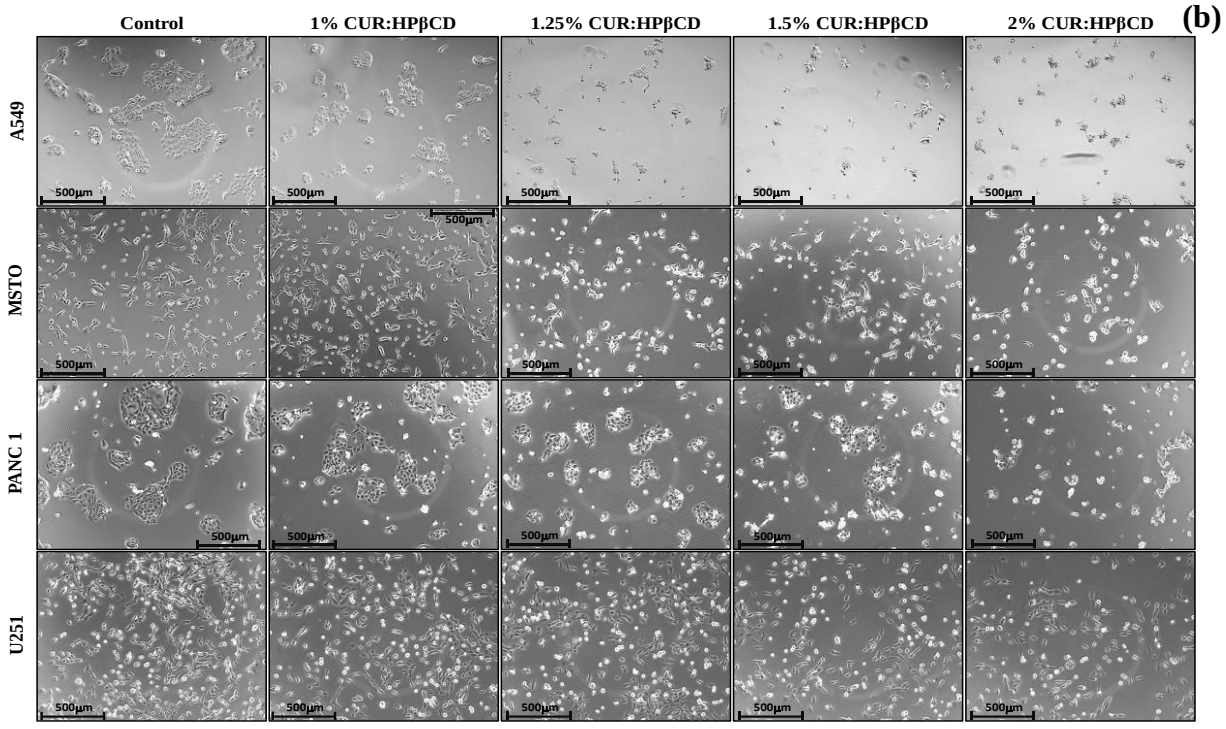
Control
1% CUR:HPβCD
1.25% CUR:HPβCD
1.5% CUR:HPβCD
2% CUR:HPβCD
A549
MSTO
PANC 1
U251
500µm
(b)

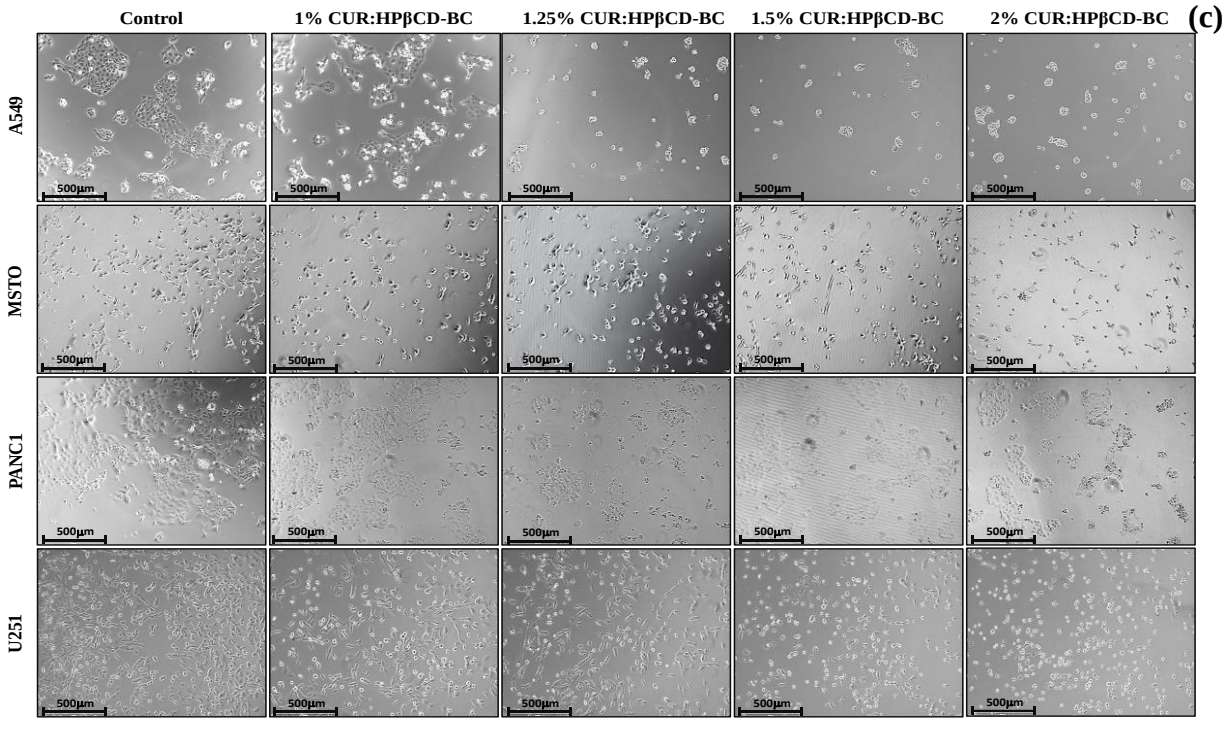
Control
1% CUR:HPβCD-BC
1.25% CUR:HPβCD-BC
1.5% CUR:HPβCD-BC
2% CUR:HPβCD-BC
A549
MSTO
PANC1
U251
500µm
(c)

Figure 9: Cytocompatibility test results. Bar graphs showing viability of different cells after 24 h exposure to **(a)** free CUR:HPβCD and 2 % CUR:HPβCD-loaded-BC. Representative optical photomicrographs of cells captured at 10x magnification after exposure for 24 h to **(b)** free CUR:HPβCD **(c)** 2 % CUR:HPβCD-loaded-BC.

3.3.2. CUR release and Antimicrobial study

CUR release from CUR:HPβCD-loaded-BC hydrogels, as determined by UV-Vis spectroscopy, is presented in Fig. 10. Results indicate that 76.99±4.46 % release (n=6) was achieved after 6 h from CUR:HPβCD-loaded-BC hydrogels. The release was slow after this duration and reached 79.36± 4.71 % at 24 h. The maximum release achieved at 48 h was 82.19±4.75 % confirming high bioavailability of CUR:HPβCD at the wound site to control bacterial infection during the treatment period.

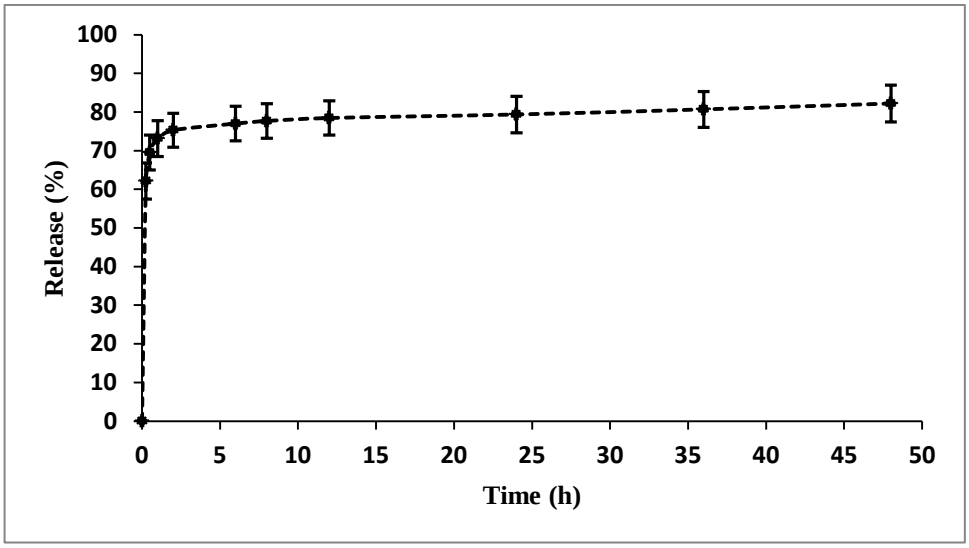

Figure 10: Release profile over 48 h from CUR:HPβCD-loaded-BC hydrogels (n=6; error bars = SD).

After the release profile was evaluated, the disc diffusion assay was undertaken to assess the antimicrobial activity of CUR:HPβCD-loaded-BC hydrogels. The results revealed no anti-microbial activity against *S. aureus* (Gram positive) for neat BC and HPβCD-loaded-BC which is in accordance with literature [7,25,50,51]. However, CUR:HPβCD-loaded-BC hydrogels demonstrated significant ($p<0.01$) antimicrobial activity (Fig. 11) (ZOI= 11.08±0.90 mm) (n=12) compared to neat BC and HPβCD-loaded-BC. CUR is well known for its antimicrobial properties against a broad range of microorganisms [52-54]. Its antimicrobial activity ensues due to its ability to interact with an essential prokaryotic cell division initiating protein (FtsZ)

[54,55]. Moreover, it has been identified to possess inhibitory effect against sortase A, a membrane-associated transpeptidase that plays a crucial role in modulating the ability of Gram-positive bacteria (including *S. aureus*) to adhere to the host tissue and cause infection [53]. The disc diffusion results confirmed that CUR maintained it antimicrobial feature even after encapsulation in the HPβCD cavity demonstrating the potential use of CUR:HPβCD as an antimicrobial for wound management.

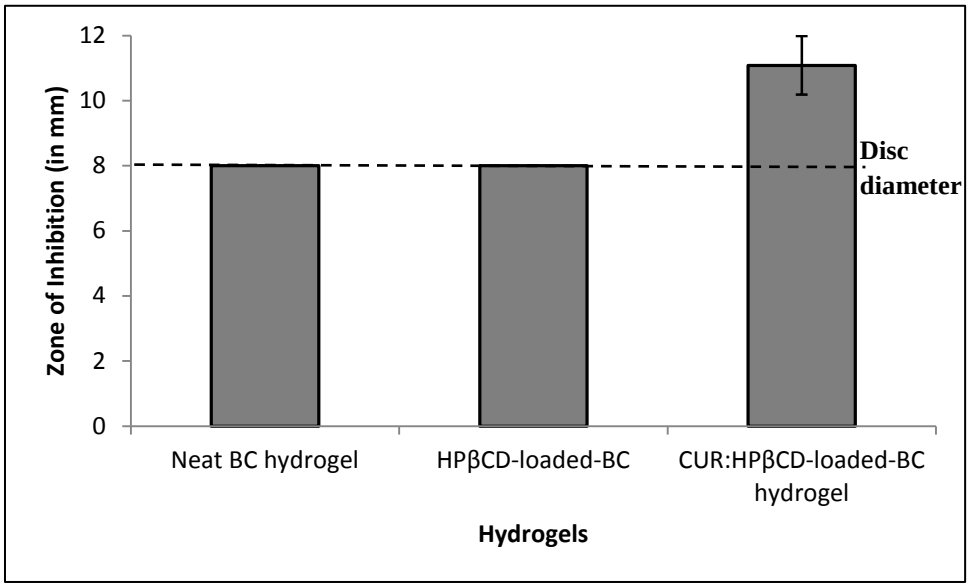

Figure 11: Antimicrobial activity assessed by ZOI during the disc diffusion assay for neat BC hydrogel, HPβCD-loaded-BC and CUR:HPβCD-loaded-BC hydrogels against *S. aureus* (n=12; error bars = SD).

3.3.3. Anti-oxidant activity by DPPH assay

Oxidative stress has been identified, through preclinical and clinical studies, as one of the major causes of nonhealing in chronic wounds [56]. CUR is reported as a potent antioxidant due to its ability to reduce reactive oxygen species such as super oxide radicals, lipid peroxyl radicals and hydroxyl radicals [10,57]. Its antioxidant activity arises due to its ability to undergo H-atom abstraction from its phenol groups giving rise to a stable, delocalised radical species [56]. Several methods have been adopted to assess the free radical scavenging potential of anti-oxidant substance and the DPPH assay is still one of the routinely practiced method for this assessment. In the current study, the antioxidant activity of CUR:HPβCD was assessed by this assay. The reaction of DPPH radicals with antioxidant is a kinetic driven process which varies for different antioxidants. In the current study, a fixed reaction time mode of 30 min was adopted for estimation of the antioxidant activity [58].

The percent antioxidant effect for supramolecular CUR:HPβCD against DPPH determined in the current study ranged from 12.06±0.014 - 79.75±0.001 % in the range of 125-2000 µg/mL and the IC_{50} was found to be 1087.49±6.47 µg/mL (n=3). It was found that HPβCD does not have antioxidant activity and our results are in agreement with literature [59]. These finding confirmed that the antioxidant activity of CUR stays preserved even after its encapsulation in HPβCD cavity in the CUR:HPβCD inclusion complex. These findings are in accordance with Aytac & Uyar (2017) [34]. These results advocate the antioxidant potential of BC hydrogels loaded with CUR:HPβCD to reduce the oxidative stress at the impaired wound site.

4. Conclusion:

The present study demonstrates the production, physicochemical characterisation, *in vitro* biocompatibility and antimicrobial performance of biosynthetic CUR:HPβCD-loaded-BC hydrogels for potential wound management applications. The physicochemical characterisation confirmed the formation of IC of CUR:HPβCD with enhanced aqueous solubility compared to free CUR. Varying the solvent volume ratios during the solvent evaporation method, IC 75 emerged to be the best preparation method with the highest encapsulation efficacy. The CUR:HPβCD-loaded-BC hydrogels demonstrated high light transmission, a property that has a potential of clinical wound monitoring without the need to remove the dressing. Moreover, these hydrogels offer optimum WVTR that could help maintain the moist environment at the wound site. Their high moisture content, biocompatibility (cytocompatibility and haemocompatibility), antimicrobial and antioxidant properties advocates their potential application as hydrogel dressings for chronic, infected wound management. These findings suggest that biosynthetic CUR:HPβCD-loaded-BC hydrogels could represent an alternative in the dressing landscape for wound management.

Acknowledgement:

The authors would like to thank Brian Johnston, Kate Butcher and Surila Darbar for their kind assistance. This research was partially supported by the European Regional Development Fund Project EnTRESS No 01R16P00718. Abhishek Gupta would like to thank the University of Wolverhampton for financial support for his PhD research.

Conflict of interest

The authors confirm no conflict of interest. The authors alone are responsible for the content and writing of the article.

Appendix A. Supporting material

Supplementary material related to this article can be found in this section.

5. References

1. A. Gupta, M. Kowalczuk, W. Heaselgrave, S.T. Britland, C. Martin, I. Radecka, The production and application of hydrogels for wound management: A review, Eur. Polym. J. 111 (2019) 134–151. doi:10.1016/j.eurpolymj.2018.12.019.
2. C. Martin, W. Low, A. Gupta, M. Amin, I. Radecka, S. Britland, P. Raj, K. Kenward, Strategies for Antimicrobial Drug Delivery to Biofilm, Curr. Pharm. Des. 21 (2014) 43–66. doi:10.2174/1381612820666140905123529.
3. K. Vowden, P. Vowden, Wound dressings: principles and practice, Surg. 35 (2017) 489–494. doi:10.1016/j.mpsur.2017.06.005.
4. T. Abdelrahman, H. Newton, Wound dressings: principles and practice, Surg. 29 (2011) 491–495. doi:10.1016/j.mpsur.2011.06.007.
5. G.D. Winter, Formation of the Scab and the Rate of Epithelization of Superficial Wounds in the Skin of the Young Domestic Pig, Nature. 193 (1962) 293–294. doi:10.1038/193293a0.
6. J. Koehler, F.P. Brandl, A.M. Goepferich, Hydrogel wound dressings for bioactive treatment of acute and chronic wounds, Eur. Polym. J. 100 (2018) 1–11. doi:10.1016/j.eurpolymj.2017.12.046.
7. A. Gupta, W.L. Low, I. Radecka, S.T. Britland, M. Mohd Amin Cairul Iqbal, C. Martin, Characterisation and in vitro antimicrobial activity of biosynthetic silver-loaded bacterial cellulose hydrogels, J. Microencapsul. 33 (2016) 725–734. doi:10.1080/02652048.2016.1253796.
8. H. Hamedi, S. Moradi, S.M. Hudson, A.E. Tonelli, Chitosan based hydrogels and their applications for drug delivery in wound dressings: A review, Carbohydr. Polym. 199 (2018) 445–460. doi:10.1016/j.carbpol.2018.06.114.
9. D. Zmejkoski, D. Spasojević, I. Orlovska, N. Kozyrovska, M. Soković, J. Glamočlija, S. Dmitrović, B. Matović, N. Tasić, V. Maksimović, M. Sosnin, K. Radotić, Bacterial cellulose-lignin composite hydrogel as a promising agent in chronic wound healing, Int. J. Biol. Macromol. 118 (2018) 494–503. doi:10.1016/j.ijbiomac.2018.06.067.
10. D. Akbik, M. Ghadiri, W. Chrzanowski, R. Rohanizadeh, Curcumin as a wound healing agent, Life Sci. 116 (2014) 1–7. doi:10.1016/j.lfs.2014.08.016.
11. A.E. Krausz, B.L. Adler, V. Cabral, M. Navati, J. Doerner, R.A. Charafeddine, D. Chandra, H. Liang, L. Gunther, A. Clendaniel, S. Harper, J.M. Friedman, J.D. Nosanchuk, A.J. Friedman, Curcumin-encapsulated nanoparticles as innovative antimicrobial and wound healing agent, Nanomedicine Nanotechnology, Biol. Med. 11 (2015) 195–206. doi:10.1016/j.nano.2014.09.004.
12. N. Wathoni, K. Motoyama, T. Higashi, M. Okajima, T. Kaneko, H. Arima, Enhancement of curcumin wound healing ability by complexation with 2-hydroxypropyl-γ-cyclodextrin in sacran hydrogel film, Int. J. Biol. Macromol. 98 (2017) 268–276. doi:10.1016/j.ijbiomac.2017.01.144.
13. E.I. Paramera, S.J. Konteles, V.T. Karathanos, Stability and release properties of curcumin encapsulated in Saccharomyces cerevisiae, β-cyclodextrin and modified starch, Food Chem. 125 (2011) 913–922. doi:10.1016/j.foodchem.2010.09.071.

14. E.M. Martin Del Valle, Cyclodextrins and their uses: a review, Process Biochem. 39 (2004) 1033–1046. doi:10.1016/s0032-9592(03)00258-9.
15. S.S. Jambhekar, P. Breen, Cyclodextrins in pharmaceutical formulations I: structure and physicochemical properties, formation of complexes, and types of complex, Drug Discov. Today. 21 (2016) 356–362. doi:10.1016/j.drudis.2015.11.017.
16. G. Dufour, B. Evrard, P. de Tullio, Rapid quantification of 2-hydroxypropyl-β-cyclodextrin in liquid pharmaceutical formulations by 1H nuclear magnetic resonance spectroscopy, Eur. J. Pharm. Sci. 73 (2015) 20–28. doi:10.1016/j.ejps.2015.03.005.
17. S. V Kurkov, T. Loftsson, Cyclodextrins, Int. J. Pharm. 453 (2013) 167–180. doi:10.1016/j.ijpharm.2012.06.055.
18. M.M. Yallapu, M. Jaggi, S.C. Chauhan, β-Cyclodextrin-curcumin self-assembly enhances curcumin delivery in prostate cancer cells, Colloids Surfaces B Biointerfaces. 79 (2010) 113–125. doi:10.1016/j.colsurfb.2010.03.039.
19. P.R.K. Mohan, G. Sreelakshmi, C. V Muraleedharan, R. Joseph, Water soluble complexes of curcumin with cyclodextrins: Characterization by FT-Raman spectroscopy, Vib. Spectrosc. 62 (2012) 77–84. doi:10.1016/j.vibspec.2012.05.002.
20. S. Hestrin, M. Schramm, Synthesis of cellulose byAcetobacter xylinum. 2. Preparation of freeze-dried cells capable of polymerizing glucose to cellulose, Biochem. J. 58 (1954) 345–352. doi:10.1042/bj0580345.
21. C. Jantarat, P. Sirathanarun, S. Ratanapongsai, P. Watcharakan, S. Sunyapong, A. Wadu, Curcumin-Hydroxypropyl-β-Cyclodextrin Inclusion Complex Preparation Methods: Effect of Common Solvent Evaporation, Freeze Drying, and pH Shift on Solubility and Stability of Curcumin, Trop. J. Pharm. Res. 13 (2014) 1215. doi:10.4314/tjpr.v13i8.4.
22. H.E. Gottlieb, V. Kotlyar, A. Nudelman, NMR Chemical Shifts of Common Laboratory Solvents as Trace Impurities, J. Org. Chem. 62 (1997) 7512–7515. doi:10.1021/jo971176v.
23. ASTM E96 / E96M-16. Standard Test Methods for Water Vapor Transmission of Materials, 2016.
24. S. Hu, X. Cai, X. Qu, B. Yu, C. Yan, J. Yang, F. Li, Y. Zheng, X. Shi, Preparation of biocompatible wound dressings with long-term antimicrobial activity through covalent bonding of antibiotic agents to natural polymers, Int. J. Biol. Macromol. 123 (2019) 1320–1330. doi:10.1016/j.ijbiomac.2018.09.122.
25. A. Gupta, W.L. Low, S.T. Britland, I. Radecka, C. Martin, Physicochemical characterisation of biosynthetic bacterial cellulose as a potential wound dressing material, British J. Phar. 2 (2017) S37-38. doi: 10.5920/bjpharm.2017.27.
26. L.-O. Lamke, G.E. Nilsson, H.L. Reithner, The evaporative water loss from burns and the water-vapour permeability of grafts and artificial membranes used in the treatment of burns, Burns. 3 (1977) 159–165. doi:10.1016/0305-4179(77)90004-3.
27. B. Balakrishnan, M. Mohanty, P. umashankar, A. Jayakrishnan, Evaluation of an in situ forming hydrogel wound dressing based on oxidized alginate and gelatin, Biomaterials. 26 (2005) 6335–6342. doi:10.1016/j.biomaterials.2005.04.012.
28. T. Takao, F. Kitatani, N. Watanabe, A. Yagi, K. Sakata, A Simple Screening Method for Antioxidants and Isolation of Several Antioxidants Produced by Marine Bacteria from Fish and Shellfish, Biosci. Biotechnol. Biochem. 58 (1994) 1780–1783. doi:10.1271/bbb.58.1780.

29. Z. Chen, R. Bertin, G. Froldi, EC50 estimation of antioxidant activity in DPPH assay using several statistical programs, Food Chem. 138 (2013) 414–420. doi:10.1016/j.foodchem.2012.11.001.
30. L. Zhao, L. Kang, Y. Chen, G. Li, L. Wang, C. Hu, P. Yang, Spectral study on conformation switchable cationic calix[4]carbazole serving as curcumin container, stabilizer and sustained-delivery carrier, Spectrochim. Acta Part A Mol. Biomol. Spectrosc. 193 (2018) 276–282. doi:10.1016/j.saa.2017.12.037.
31. Y. Sun, L. Du, Y. Liu, X. Li, M. Li, Y. Jin, X. Qian, Transdermal delivery of the in situ hydrogels of curcumin and its inclusion complexes of hydroxypropyl-β-cyclodextrin for melanoma treatment, Int. J. Pharm. 469 (2014) 31–39. doi:10.1016/j.ijpharm.2014.04.039.
32. N. Li, N. Wang, T. Wu, C. Qiu, X. Wang, S. Jiang, Z. Zhang, T. Liu, C. Wei, T. Wang, Preparation of curcumin-hydroxypropyl-β-cyclodextrin inclusion complex by cosolvency-lyophilization procedure to enhance oral bioavailability of the drug, Drug Dev. Ind. Pharm. 44 (2018) 1966–1974. doi:10.1080/03639045.2018.1505904.
33. A. Radjaram, A.F. Hafid, D. Setyawan, Dissolution enhancement of curcumin by hydroxypropyl-β-cyclodextrin complexation. Int. J. Phar. and Pharma. Sci. 5, (2013) 401-405.
34. Z. Aytac, T. Uyar, Core-shell nanofibers of curcumin/cyclodextrin inclusion complex and polylactic acid: Enhanced water solubility and slow release of curcumin, Int. J. Pharm. 518 (2017) 177–184. doi:10.1016/j.ijpharm.2016.12.061.
35. C.-M. Hsu, S.-C. Yu, F.-J. Tsai, Y. Tsai, Enhancement of rhubarb extract solubility and bioactivity by 2-hydroxypropyl-β-cyclodextrin, Carbohydr. Polym. 98 (2013) 1422–1429. doi:10.1016/j.carbpol.2013.07.029.

36. P. Mura, Analytical techniques for characterization of cyclodextrin complexes in the solid state: A review, J. Pharm. Biomed. Anal. 113 (2015) 226–238. doi:10.1016/j.jpba.2015.01.058.
37. Z. Di, Z. Shi, M.W. Ullah, S. Li, G. Yang, A transparent wound dressing based on bacterial cellulose whisker and poly(2-hydroxyethyl methacrylate), Int. J. Biol. Macromol. 105 (2017) 638–644. doi:10.1016/j.ijbiomac.2017.07.075.
38. S. Tyeb, N. Kumar, A. Kumar, V. Verma, Flexible agar-sericin hydrogel film dressing for chronic wounds, Carbohydr. Polym. 200 (2018) 572–582. doi:10.1016/j.carbpol.2018.08.030.
39. H. Zhang, X. Luo, H. Tang, M. Zheng, F. Huang, A novel candidate for wound dressing: Transparent porous maghemite/cellulose nanocomposite membranes with controlled release of doxorubicin from a simple approach, Mater. Sci. Eng. C. 79 (2017) 84–92. doi:10.1016/j.msec.2017.05.019.
40. H. Shahbazi, M. Tataei, M.H. Enayati, A. Shafeiey, M.A. Malekabadi, Structure-transmittance relationship in transparent ceramics, J. Alloys Compd. 785 (2019) 260–285. doi:10.1016/j.jallcom.2019.01.124.
41. Z. Tehrani, H.R. Nordli, B. Pukstad, D.T. Gethin, G. Chinga-Carrasco, Translucent and ductile nanocellulose-PEG bionanocomposites—A novel substrate with potential to be

functionalized by printing for wound dressing applications, Ind. Crops Prod. 93 (2016) 193–202. doi:10.1016/j.indcrop.2016.02.024.

42. H. Adeli, M.T. Khorasani, M. Parvazinia, Wound dressing based on electrospun PVA/chitosan/starch nanofibrous mats: Fabrication, antibacterial and cytocompatibility evaluation and in vitro healing assay, Int. J. Biol. Macromol. 122 (2019) 238–254. doi:10.1016/j.ijbiomac.2018.10.115.
43. ASTM F756-17. Standard Practice for Assessment of Hemolytic Properties of Materials. 2017
44. E.A. Kamoun, E.-R.S. Kenawy, T.M. Tamer, M. El-Meligy, M.S. Mohy Eldin, Poly (vinyl alcohol)-alginate physically crosslinked hydrogel membranes for wound dressing applications: Characterization and bio-evaluation, Arab. J. Chem. 8 (2015) 38–47. doi:10.1016/j.arabjc.2013.12.003.
45. M.E. Hiro, Y.N. Pierpont, F. Ko, T.E. Wright, M.C. Robson, W.G. Payne, Comparative evaluation of silver-containing antimicrobial dressings on in vitro and in vivo processes of wound healing. Eplasty 12 (2012) 409-419.
46. S.-B. Zou, W.-Y. Yoon, S.-K. Han, S.-H. Jeong, Z.-J. Cui, W.-K. Kim, Cytotoxicity of silver dressings on diabetic fibroblasts, Int. Wound J. 10 (2012) 306–312. doi:10.1111/j.1742-481x.2012.00977.x.
47. M. Amirthalingam, N. Kasinathan, S. Mutalik, N. Udupa, In vitrobiocompatibility and release of curcumin from curcumin microcomplex-loaded chitosan scaffold, J. Microencapsul. 32 (2015) 364–371. doi:10.3109/02652048.2015.1028496.
48. A. Kurniawan, F. Gunawan, A.T. Nugraha, S. Ismadji, M.-J. Wang, Biocompatibility and drug release behavior of curcumin conjugated gold nanoparticles from aminosilane-functionalized electrospun poly(N -vinyl-2-pyrrolidone) fibers, Int. J. Pharm. 516 (2017) 158–169. doi:10.1016/j.ijpharm.2016.10.067.
49. X. Liu, L. You, S. Tarafder, L. Zou, Z. Fang, J. Chen, C.H. Lee, Q. Zhang, Curcumin-releasing chitosan/aloe membrane for skin regeneration, Chem. Eng. J. 359 (2019) 1111–1119. doi:10.1016/j.cej.2018.11.073

50. G. Yang, J. Xie, F. Hong, Z. Cao, X. Yang, Antimicrobial activity of silver nanoparticle impregnated bacterial cellulose membrane: Effect of fermentation carbon sources of bacterial cellulose, Carbohydr. Polym. 87 (2012) 839–845. doi:10.1016/j.carbpol.2011.08.079.
51. O. Aleem, B. Kuchekar, Y. Pore, S. Late, Effect of β-cyclodextrin and hydroxypropyl β-cyclodextrin complexation on physicochemical properties and antimicrobial activity of cefdinir, J. Pharm. Biomed. Anal. 47 (2008) 535–540. doi:10.1016/j.jpba.2008.02.006.
52. S.-H. Mun, D.-K. Joung, Y.-S. Kim, O.-H. Kang, S.-B. Kim, Y.-S. Seo, Y.-C. Kim, D.-S. Lee, D.-W. Shin, K.-T. Kweon, D.-Y. Kwon, Synergistic antibacterial effect of curcumin against methicillin-resistant Staphylococcus aureus, Phytomedicine. 20 (2013) 714–718. doi:10.1016/j.phymed.2013.02.006.

53. P. Hu, P. Huang, M.W. Chen, Curcumin reduces Streptococcus mutans biofilm formation by inhibiting sortase A activity, Arch. Oral Biol. 58 (2013) 1343–1348. doi:10.1016/j.archoralbio.2013.05.004.
54. A.C. da Silva, P.D. de F. Santos, J.T. do P. Silva, F.V. Leimann, L. Bracht, O.H. Gonçalves, Impact of curcumin nanoformulation on its antimicrobial activity, Trends Food Sci. Technol. 72 (2018) 74–82. doi:10.1016/j.tifs.2017.12.004.
55. D. Rai, J.K. Singh, N. Roy, D. Panda, Curcumin inhibits FtsZ assembly: an attractive mechanism for its antibacterial activity, Biochem. J. 410 (2008) 147–155. doi:10.1042/bj20070891.
56. C. Mohanty, S.K. Sahoo, Curcumin and its topical formulations for wound healing applications, Drug Discov. Today. 22 (2017) 1582–1592. doi:10.1016/j.drudis.2017.07.001
57. S. Jena, C. Anand, G.B.N. Chainy, J. Dandapat, Induction of oxidative stress and inhibition of superoxide dismutase expression in rat cerebral cortex and cerebellum by PTU-induced hypothyroidism and its reversal by curcumin, Neurol. Sci. 33 (2011) 869–873. doi:10.1007/s10072-011-0853-4.

58. K. Mishra, H. Ojha, N.K. Chaudhury, Estimation of antiradical properties of antioxidants using DPPH assay: A critical review and results, Food Chem. 130 (2012) 1036–1043. doi:10.1016/j.foodchem.2011.07.127.
59. J. Rakmai, B. Cheirsilp, J.C. Mejuto, J. Simal-Gándara, A. Torrado-Agrasar, Antioxidant and antimicrobial properties of encapsulated guava leaf oil in hydroxypropyl-beta-cyclodextrin, Ind. Crops Prod. 111 (2018) 219–225. doi:10.1016/j.indcrop.2017.10.027.

Supporting information

Figure S1 a: Chemical structure of curcumin (CUR) with annotations for NMR assignments.

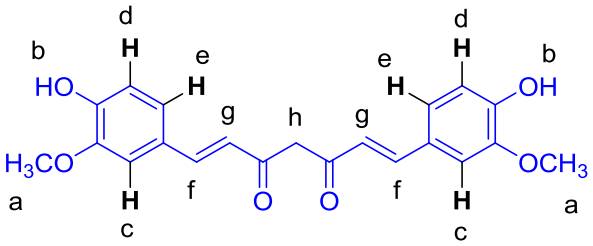

Figure S1 b: Chemical structure and a truncated cone schematic of hydroxylpropyl-β-cyclodextrin (HPβCD). Annotations for NMR assignments are shown on one glucose unit below.

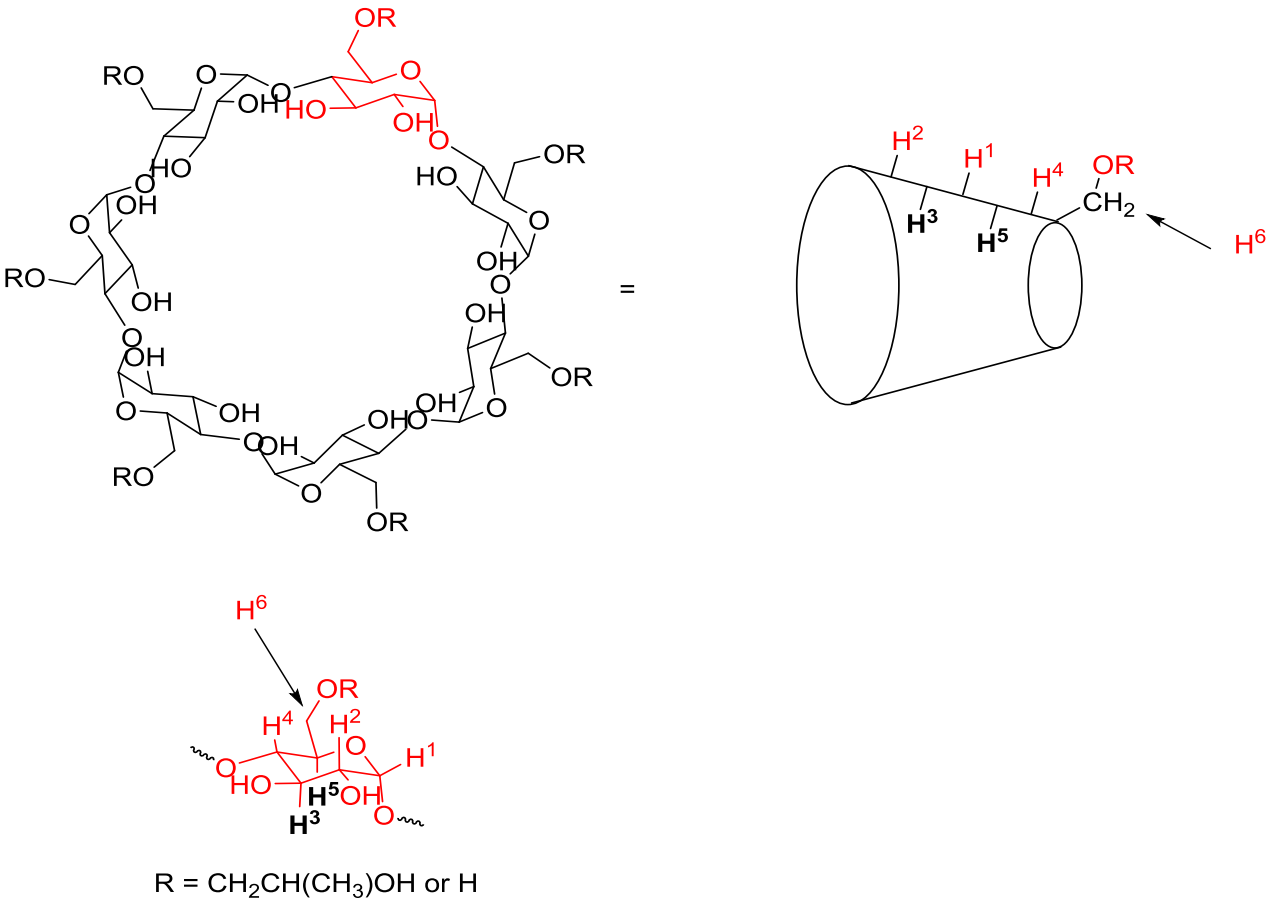

S1 c: The schematic representation of CUR:HPβCD inclusion complex. Through space ROESY correlations (cross peaks) are observed between the HPβCD internal CHs (H^3 and H^5) and the aryl CH groups of CUR (H_c, H_d and H_e). Note: only one of seven glucose units included in annotation.

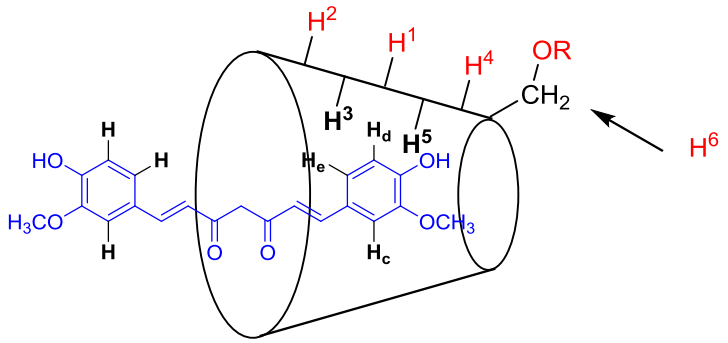

NMR analysis of inclusion complex

Figure S2: ^{1}H NMR of the CUR:HPβCD inclusion complex in D_2O

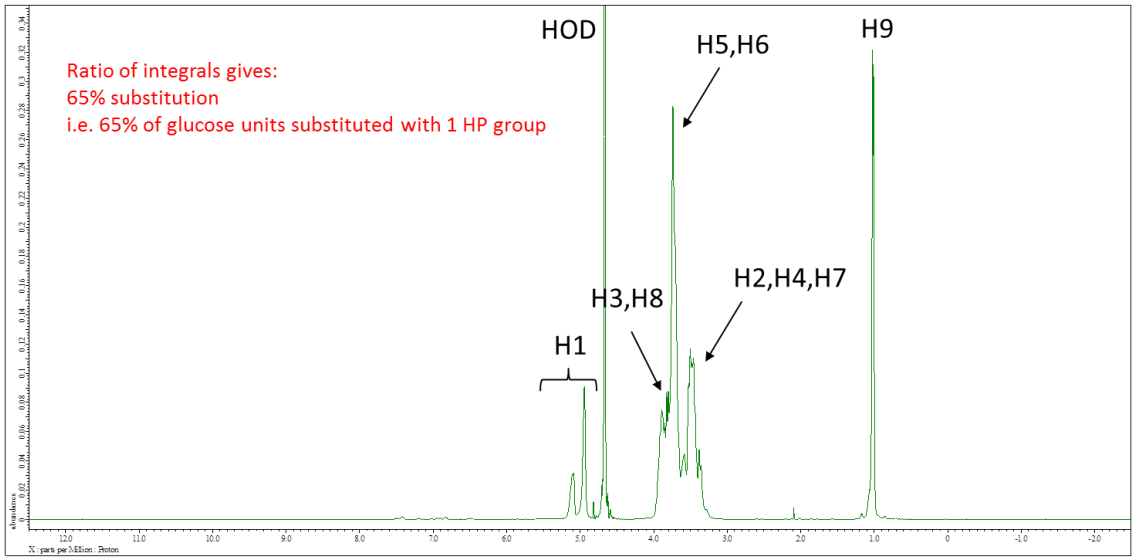

Figure S3: Expansion of ^{1}H NMR of the CUR:HPβCD inclusion complex in D_2O

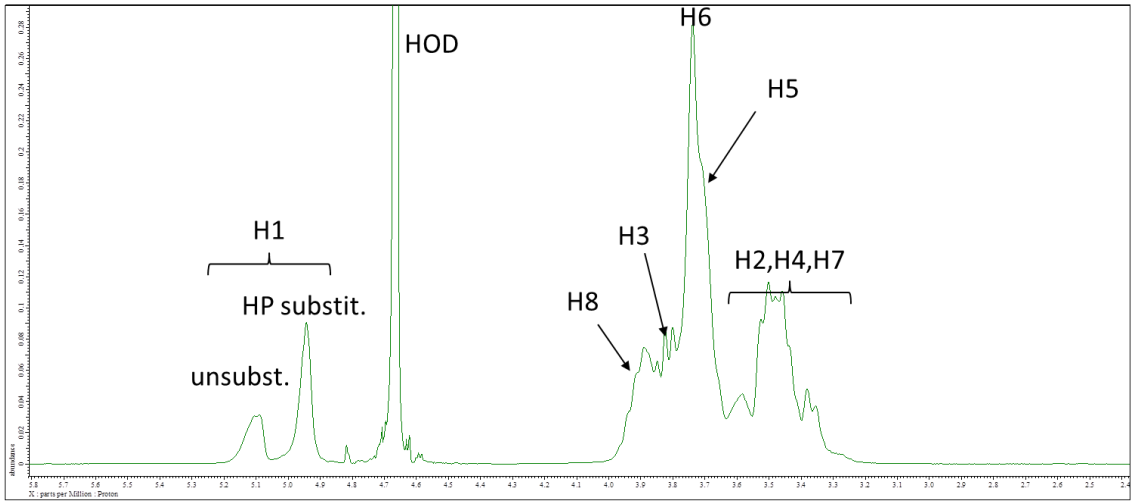

Figure S4: ^{13}C NMR of the CUR:HPβCD inclusion complex in D_2O

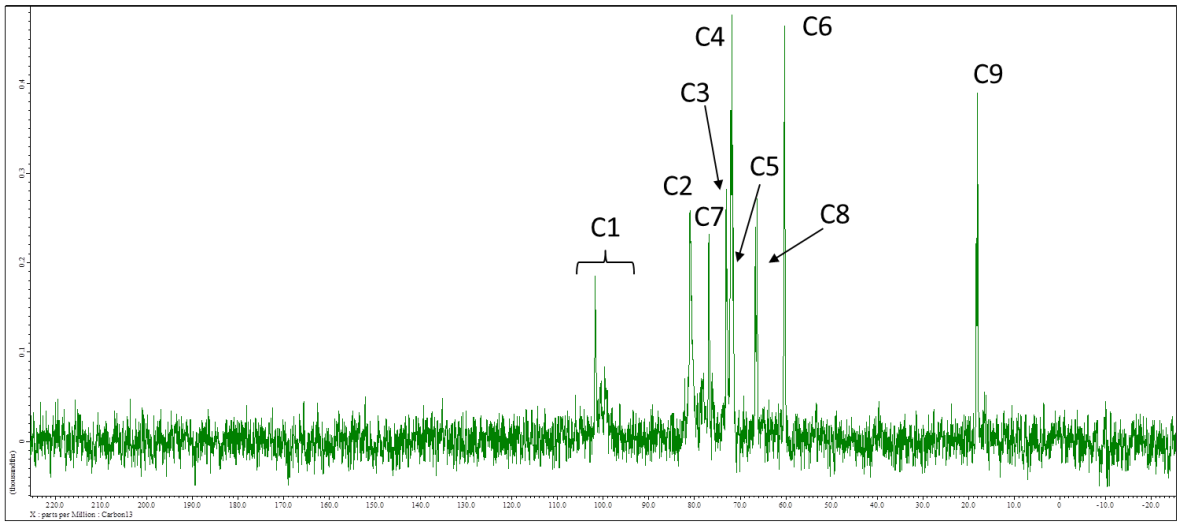

Assignments from HSQC and HMBC

Figure S5: Expansion of ^{13}C NMR of the CUR:HPβCD inclusion complex in D_2O

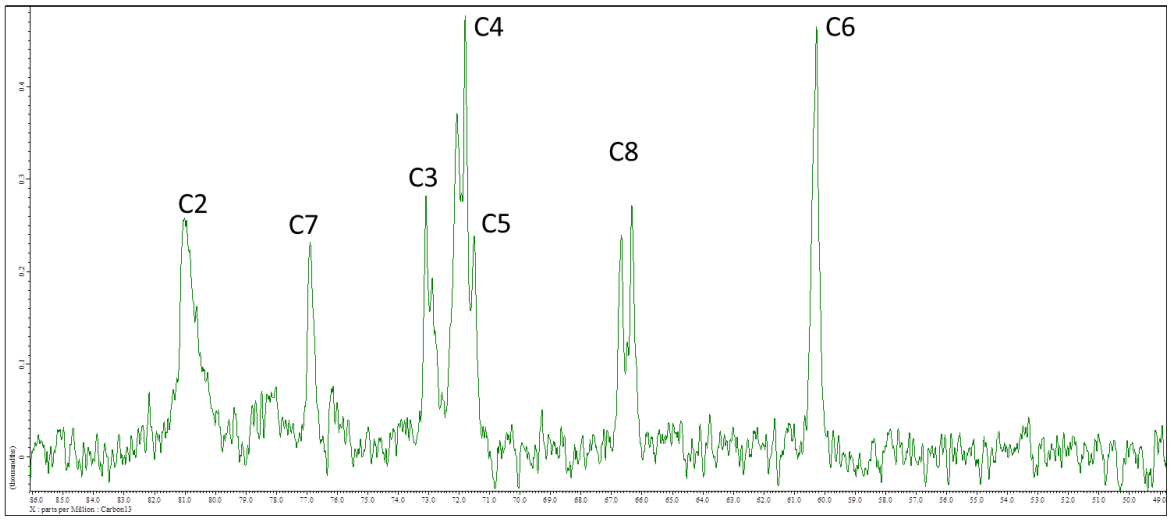

NB: Some peaks "doubled" due to 65% substitution of HP groups

Figure S6: Overlay of ^{1}H spectra of HPβCD and the CUR:HPβCD inclusion complex in D_2O

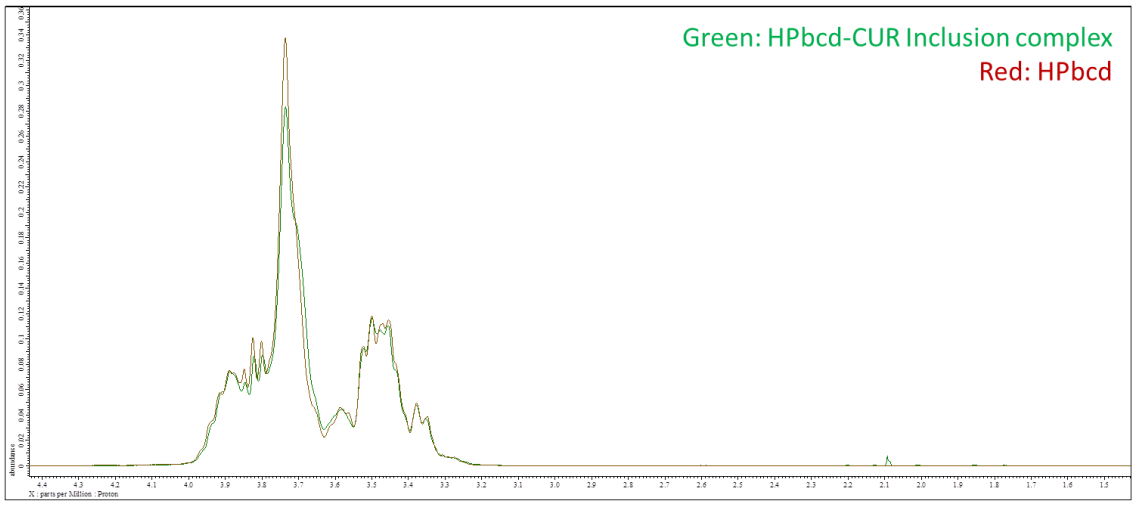

Figure S7: Expansion overlay of ^{1}H spectra of HPβCD and the CUR:HPβCD inclusion complex in D_2O